AGU100 ADVANCING EARTH AND SPACE SCIENCE

Water Resources Research

RESEARCH ARTICLE
10.1029/2017WR021242

**Key Points:**
- A new method of using transit time distributions of discharge and evaporation to help identify lake mixing and flow paths
- Evaporation flux ages are much younger than lake outflows, drawing primarily on young summer inputs
- Catchments influenced by lakes may yield shorter transit times due to evaporation effects

**Correspondence to:**
A. A. Smith,
aaron.smith@abdn.ac.uk

**Citation:**
Smith, A. A., Tetzlaff, D., & Soulsby, C. (2018). On the use of StorAge Selection functions to assess time-variant travel times in lakes. *Water Resources Research*, *54*, 5163–5185. https://doi.org/10.1029/2017WR021242

Received 5 JUN 2017
Accepted 22 JUN 2018
Accepted article online 10 JUL 2018
Published online 29 JUL 2018



# On the Use of StorAge Selection Functions to Assess Time-Variant Travel Times in Lakes

**A. A. Smith[1], D. Tetzlaff[1,2,3], and C. Soulsby[1]**

[1]Northern Rivers Institute, School of Geosciences, University of Aberdeen, UK, [2]IGB Leibniz Institute of Freshwater Ecology and Inland Fisheries Berlin, Berlin, Germany, [3]Department of Geography, Humbolt University Berlin, Berlin, Germany

**Abstract** Lakes can store water for long periods of time, which influences the transport of water and hydrologic tracers and changes catchment transit times downstream. However, the impact that the transit time of lakes has on catchment transit times has received little attention to date. We derived water and isotope mass balances for two lakes and examine the use of time-variant transit time solutions with StorAge Selection functions to estimate the water ages of evaporation and lake outflows. We used the convolution of the StorAge Selection function transit time estimations with inflow transit times to estimate the transit times downstream of each lake. The lakes exhibited contrasting storage effects for discharge; with direct storage effects (newest water exiting during low flow) for a larger lake fed by a small catchment, and inverse storage effects (newest water exiting during high flow) for a smaller lake with a large catchment. The water and isotope mass balance yielded estimates of daily and annual evaporation fluxes, which were similar between the two lakes. The proposed framework is an effective tool to identify the effects of precipitation, surface inflow, and evaporation on the transit times for relatively small, shallow lakes, using a combination of water and isotope mass balance methods.

## 1. Introduction

Catchment transit time modeling using environmental tracers provides valuable insights into dominant water flow paths and ages in a parsimonious manner (Kirchner et al., 2001). For this reason, transit time distributions (TTDs) have been widely used in areas of both high and low topographic relief (e.g., Asano et al., 2002; Soulsby et al., 2000), tropical (e.g., Birkel et al., 2016; Muñoz-Villers et al., 2016) and semiarid areas (e.g., Ameli & Creed, 2017; Hrachowitz et al., 2011), and catchments with seasonally variable precipitation (i.e., snowfall and rainfall; e.g., Maloszewski et al., 1992; Rodgers et al., 2005). While catchment-scale TTD modeling has been extensively explored with time-invariant approaches, there is a deficiency of studies on the effect of lakes on catchment-scale TTDs. Travel time estimation for catchments with lakes can be complex as the transit time in lakes may disrupt the smooth shape of the catchment TTD by attenuating the peaks of input fluxes, contributing large volumes of evaporation, and providing potentially different flow mechanisms. While transit time mapping and routing in lakes has previously been used to help identify fast and slow flow paths within a stratified system (e.g., Kalinin et al., 2016), the effect of the lakes on the catchment transit time has not been assessed. The limited assessment of lakes on catchment TTDs in travel time studies is a particular concern for catchments in northern latitudes that have a higher proportion of lakes per unit area than catchments in middle or southerly latitudes (Messager et al., 2016). This complicates the quantification of catchment transport and restricts transit time estimations in a region where hydrologic measurements are limited (Laudon et al., 2017). It has also been shown that lake evaporation may have an important influence on transit time estimations within tracer-aided models, particularly when considering water isotope tracers (Birkel et al., 2011b). Some attempts have been made to include lakes into catchment transit time analysis by integrating land cover characteristics with stable isotopes to quantify potential changes in the mean transit time (MTT) in catchments affected by regulation for hydropower generation (Soulsby, Birkel, Geris, Dick, et al., 2015).

In recent attempts to decipher transit time estimations, time-variant parameters have been used in the governing equations to assess how the MTT may change in time (Birkel et al., 2012; Hrachowitz, Soulsby, Tetzlaff, Malcolm, & Schoups, 2010). Alternative solutions of catchment storage mass balance have also assessed the time variance of MTTs by implicitly using parcel accounting to track water ages and assign the probability of water leaving storage at each time via a StorAge Selection (SAS) function (Botter et al.,

2011). Time-variant TTDs in catchments have been used for investigation of conceptual partial mixing processes (Hrachowitz et al., 2013; van der Velde et al., 2012; van der Velde et al., 2015), assessment of effective storage in catchment transport processes (Harman, 2015), constraining transit time estimations with high resolution data (Benettin et al., 2017), and the changes in flow pathway partitions and flow rate on TTD shapes and SAS functions (Heidbüchel et al., 2012, 2013; Kim et al., 2016; Pangle et al., 2017). To reduce incorrect inferences of transit time estimations caused by the effect of evaporation within the conservative mixing of the tracers, evaporation has also been considered in time-variant methods through evapoconcentration (Botter, 2012; Botter et al., 2010; Harman, 2015; Queloz et al., 2015) and fractionation (Benettin et al., 2017). The most recent advances in time-variant transit time estimations have been applications explicitly linked to catchments with changing storage conditions (Rinaldo et al., 2015), but these have yet to be applied to other smaller storage compartments such as lakes.

The conceptualization of SAS functions with the consideration of evaporation, transit time, and residence time, is potentially well suited to lake transit time estimations where changes in storage may account for time-variable mixing processes. In lakes, the effect of lake evaporation on the isotopic composition of catchment outflow is largely influenced by the rate of evaporation relative to the outflow (Froehlich et al., 2005; Gat, 1995, 2010). The evaporative fractionation results in a deviation from the composition of precipitation, and greater enrichment of heavier isotopes. The nonconservative nature of stable isotopes during evaporation also creates a potential opportunity for improved evaporation estimation (Gibson, 2002; Gibson et al., 1993; Gibson & Edwards, 1996). The versatility of SAS functions to estimate both transit and residence times is extremely useful, where transit time is the age of water leaving a lake at a given point in time and the residence time is the time water spends in a lake. The separation of these two metrics is essential for broader understanding of the temporal variability of the role of lakes in biogeochemical cycles and their interaction with the surrounding catchment compared to in-lake processes (Anderson & Cheng, 1993; Brooks et al., 2014; Cardille et al., 2007).

The River Dee, Scotland, is the largest unregulated river in the UK and provides local drinking water for >250,000 people, and sustains an economically important Atlantic salmon fishery (Smart et al., 1998; Soulsby & Tetzlaff, 2008). We examine two lake-influenced headwater catchments of the River Dee to assess the temporal variability of transit and residence times of two lakes. This study focuses on two shallow lakes: a larger lake with a small catchment and a smaller lake with a large catchment. Different SAS functions were tested over a 2-year period with the primary objective of identifying temporal changes in lake transit and residence times. We specifically aimed to (1) assess the age of lake outflows and evaporation fluxes; (2) qualitatively assess lake mixing patterns using SAS functions; and (3) assess the perceived evaporation using stable water isotope evaporative fractionation under various mixing conditions. Additionally, this work seeks to provide a general framework for incorporating lakes in time-variant transit time estimations.

## 2. Study Area

The Dinnet Burn is located in the Cairngorms National Park in Scotland and encompasses a 54.2 $km^2$ catchment, draining into the River Dee (Figure 1). A large area of designated conservation land within the catchment (The Muir of Dinnet, 11.6 $km^2$) is undergoing forest restoration following intensive agriculture and grazing in the early nineteenth century and initial forest clearance in the Bronze Age (3,000 BP). The climate is at the transition between temperate/boreal zones, though it is subarctic at higher altitudes (>500 m), with periods of snow and freezing temperatures during the winter (Soulsby et al., 2001). The freezing temperatures occasionally result in ice formation on open water bodies. The elevation of the Dinnet Burn changes significantly from west to east, decreasing 600 m from the headwaters to the outlet. The highest and lowest elevations are underlain predominately by siliceous schists, while midelevations are associated with exposed granite batholiths (Smart et al., 1998; Speed et al., 2011). Exposed bedrock is present in the highest elevation areas (Hrachowitz, Soulsby, Tetzlaff, Malcolm, & Schoups, 2010), and bedrock fractures result in a preferential flow path for groundwater recharge (Soulsby & Tetzlaff, 2008; Speed et al., 2011). However, fractured bedrock is minimal in middle- and low-relief areas and preferential flow paths to groundwater recharge are limited (Ala-aho et al., 2017). The Dinnet Burn catchment is broadly similar to the extensively studied Bruntland Burn, approximately 8 km away. Both catchments

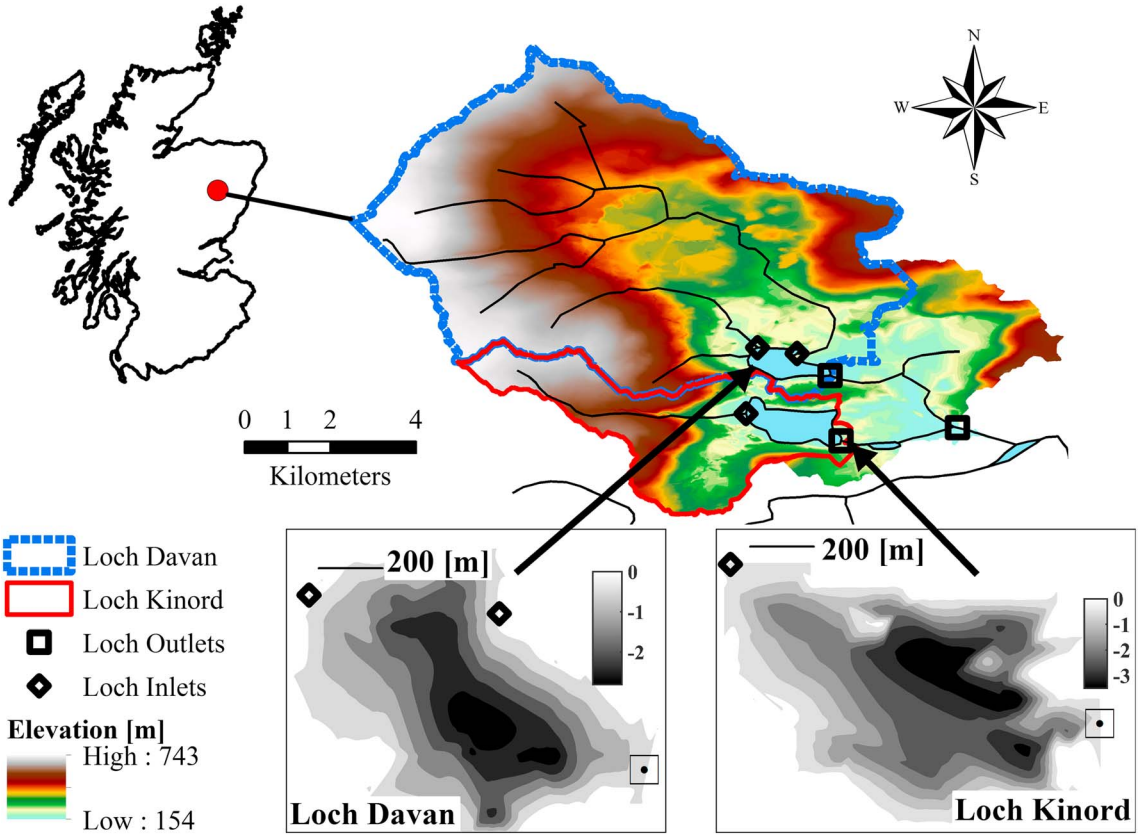


**Figure 1.** Catchments of loch Davan and loch Kinord of the Dinnet burn in NE Scotland. Bathymetric contours of each lake are displayed in meters below a datum of 0 with a spatial scale of 200 m for each lake. Major inlets (black hollow diamonds) and outlet (black hollow squares) of each lake are shown.

are generally underlain by granite and schist, characterized by steep slopes, a valley bottom lined with bogs and fens, and have virtually identical climatic regimes (Soulsby, Birkel, Geris, & Tetzlaff, 2015; Tetzlaff et al., 2014).

Below 500 m, glacial drift deposits comprising low permeability till and more freely draining alluvium, cover the underlying bedrock and result in a hummocky landscape with depressions with raised bogs and fens (Hrachowitz, Soulsby, Tetzlaff, Malcolm, & Schoups, 2010). Low permeability of the drift and glacial retreat led to the creation of two kettle holes lakes: Loch Kinord and Loch Davan. The two lakes are near the outlet of their respective catchments, with the majority of the catchment area upstream of each lake (Table 1). Loch Kinord and Loch Davan are similar in volumetric size (Table 1) to the majority of lakes in the United Kingdom (Hughes et al., 2003). The low hydraulic conductivity in the drift ($1 \cdot 10^{-8}$ m/s) in the surrounding area suggests that there is limited deep groundwater flux and the majority of lake water comes from surface water inflows (Ala-aho et al., 2017).

Loch Kinord is a large shallow lake (mean depth: 1.5 m, Figure 1) with a small upstream catchment area relative to its surface area (Table 1). The upstream catchment land cover comprised montane shrubs, conifers, open water, grassland, broad-leaf/mixed forests, and urban and agricultural usage (Table 1; CEH, 2017). Loch Kinord is a throughflow lake with continuous inflow and outflow throughout the year. There is limited variability in the lake level, which has an average level of 0.45 m and a standard deviation of 0.1 m (minimum: 0.28 m, maximum: 1.14 m; Scottish Environment Protection Agency (SEPA), 2018b). Surface water fluxes of inflow and outflow dominate the lake water balance. In Loch Kinord, surface inflow is 3 times greater than precipitation inflow.

Loch Davan is smaller but not greatly shallower than Loch Kinord (mean depth: 1.2 m, Figure 1). The upstream catchment has similar vegetation; however, there are notably fewer montane shrubs and open water areas, more grasslands areas, and urban and agricultural usage while similar proportions of conifers and broad-leaf/

**Table 1**
*Physiographic Properties of Loch Kinord and Loch Davan Catchments and Bathymetry (CEH, 2017)*

| Lake and Catchment Properties | Loch Kinord | Loch Davan |
|---|---|---|
| Inflow catchment area ($km^2$) | 8.4 | 34 |
| Catchment drainage density ($km^{-1}$) | 0.92 | 0.78 |
| Primary inflow drainage density ($km^{-1}$) | 1.01 | 0.75 |
| Secondary inflow drainage density ($km^{-1}$) | N/A | 0.72 |
| Surface area ($km^2$) | 0.77 | 0.42 |
| Volume ($m^3$) | 1,152,954 | 505,904 |
| Maximum depth (m) | 3.7 | 2.7 |
| Mean catchment elevation (meters above sea level) | 243 | 275 |
| Lake elevation (meters above sea level) | 170 | 170 |
| Land cover percentage (%) | | |
| Montane shrubs | 56 | 35 |
| Conifers | 24 | 21 |
| Open water | 8 | 1 |
| Grassland | 4 | 26 |
| Broadleaf/mixed forest | 4 | 3 |
| Urban and agriculture | 4 | 14 |

*Note.* Land cover is allocated with percentages of montane shrubs (MS), conifers (C), open water (O), grassland (G), broad-leaf/mixed forests (BF), and urban and agriculture (U). N/A = not applicable.

mixed forests to the catchment upstream of Loch Kinord (Table 1; CEH, 2017). Loch Davan is also a throughflow lake with continuous inflow provided by two surface inflows (Logie Burn is the primary inflow, and Red Burn is the secondary inflow). The surface inflows provide approximately 41 times more flow relative to precipitation.

## 3. Data and Sampling Methods

Rainfall, temperature, wind speed, net radiation, and relative humidity were measured at the Bruntland Burn experimental catchment (8 km away). Between August 2014 and August 2016, the highest precipitation occurred from November to January (>3.5 mm/day on average), while late winter (February and March), spring (May), and early autumn (September) were drier (< 2 mm/day on average; Figure 2a). The long-term average annual precipitation for the site was 1,090 mm. A comparison of the nearest precipitation stations within 10 km of the lakes (Glenshiel, Polhollick, and Bruntland Burn) have good agreement on total precipitation between August 2014 and August 2016 (1,834, 1,870, and 1,985 mm, respectively). The deviation between stations is less than 8%, which is similar to the measurement uncertainty at each station. During

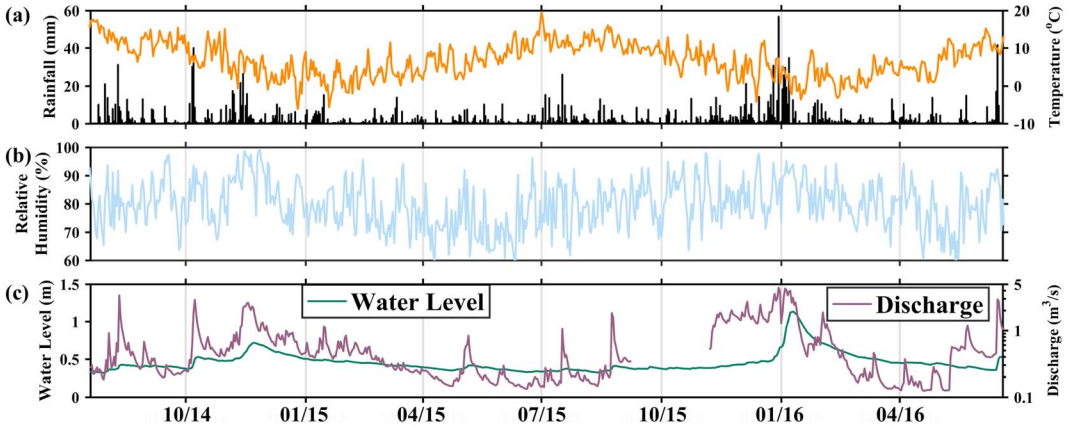


**Figure 2.** (a) Daily rainfall (mm/day) and air temperature at a weather station 8 km to the lakes, (b) daily measured relative humidity, and (c) measured water level in Loch Kinord and measured discharge flowing into Loch Davan via the largest channel (Logie Burn).

the study period there was a 1-in-200-year storm (December 2015 to early January 2016), which resulted in the largest flood on the River Dee since 1829 (Marsh et al., 2016; Soulsby et al., 2017). The event greatly increased the water level and discharge for both study lakes. Relative humidity was high with an annual mean relative humidity of 80% (Figure 2b). Air temperatures varied between ~0 °C in winter and ~14 °C in summer.

Water level in Loch Kinord has been measured at 15-min intervals at the south end of the lake since February 2008. The primary inflow to Loch Davan, the Logie Burn, drains a catchment area of ~30 $km^2$ and was the only measured streamflow to the lakes. Discharge measurements were conducted using a pressure transducer and a previously developed rating curve. Biweekly sampling of the primary surface inflows and outflows for deuterium ($^2H$) and oxygen-18 ($^{18}O$) was conducted for the first 12 months of the study period, followed by 12 months of monthly and additional opportunistic sampling during large events (e.g., December 2015 to January 2016). Precipitation was sampled daily at the Bruntland Burn (Tetzlaff et al., 2014). The measurement location at the Bruntland Burn is at approximately the same elevation (250 m above sea level) as the mean catchment elevations for Loch Kinord and Loch Davan, and less than 100 m higher than the elevation of each lake (Table 1). It was assumed that the isotopic lapse rate is insignificant due to the small elevation difference between the Bruntland Burn and the lakes. Any potential effect of elevation on precipitation isotopes is likely minimal due to the small proportion of precipitation on the lake to the total inflow (2–29%). For long-term conditions and a precipitation gradient of 1.5‰/100 m for $\delta^2H$ (Siegenthaler & Oeschger, 1980), an elevation difference of 100 m would only produce changes of inflow isotopic composition of 0.03–0.44‰ (0.03 = 1.5‰×0.02 and 0.44 = 1.5‰ ×0.29, respectively). Comparison of isotopes in precipitation at the Bruntland Burn and Lochnagar (sampled in the early 2000s, approximately 10 km from the Bruntland Burn) reveal a similar relationship between $\delta^2H$ and $\delta^{18}O$ with local meteoric water line (LMWL) slopes of 7.5 and 7.6, respectively (Tyler et al., 2007). Therefore, the relationship between $\delta^2H$ and $\delta^{18}O$ was assumed to remain the same between the Bruntland Burn and the lakes. Isotope samples were analyzed using a Los Gatos DLT-100 laser isotope analyzer (Los Gatos Research, Inc., San Jose, United States) with instrument precision of ±0.4‰ for $\delta^2H$ and ± 0.1‰ for $\delta^{18}O$. Analysis of each liquid sample involved five repeat measurements, with the initial two discarded to remove memory effects. The mean of the remaining three was taken, unless variability was greater than machine precision (±3 standard deviations), in which case samples were reanalyzed. Blanks (deionized water to reset the analyzer) and standards (five sets) were run at frequent intervals to keep lab precision equivalent to the instrument. The isotopic compositions of $\delta^2H$ and $\delta^{18}O$ are given in per mille (‰), relative to the Vienna Standard Mean Ocean Water.

## 4. Methodology

### 4.1. Lake Water Balance

For each lake, the water balance was derived with respect to changing lake volume. Bathymetry surveys for each lake were conducted prior to isotopic sampling (10 July 1905; NLS, 2017). An algorithm was developed in Matlab® to digitize the bathymetric surveys to estimate a depth-volume-surface area (D-V-A) relationship for each lake. Evidence suggests that current sedimentation in each lake is low, as the agricultural expansion in the nineteenth century was halted and replaced by conservation management and reafforestation in the twentieth century (Edwards, 1979). There is uncertainty of the D-V-A relationship relative to the measured lake level elevations due to unknown bathymetric benchmark elevations. To correlate the D-V-A relationships to the measured lake level, a lake elevation correction calibration parameter ($B_E$) was applied to the measured lake level ($D_{adj} = D_M + B_E$, where $D_M$is the measured lake level). The water balance of each lake was estimated daily using the D-V-A relationships:

$$\frac{dV(t)}{dt} = I_1(t) + I_2(t) + (P(t) - E_a(t)) \cdot A(t, V(t)) - Q(t, D(t, V(t))) \quad (1)$$

where $I$ is the surface inflow to the lake (subscript denotes the number of inflows), $P$ is the precipitation to the surface of the lake, $A$ is the lake surface area as a function of lake volume (D-V-A relationship), $Q$ is the surface water discharge from the lake as a function of lake depth, $V$ is the volume within the lake, and $E_a$ is the actual lake evaporation. Similar to the lake surface area, lake depth is a function of lake volume (D-V-A relationship). The lake volume was estimated daily using the water balance (equation (1)) for Loch Davan with two surface inflows ($I_1(t)$ and $I_2(t)$), while the water balance was modified for Loch Kinord for only one surface inflow ($I_1(t)$).

#### 4.1.1. Lake Inflow

Discharge of the largest inflow to Loch Davan (Logie Burn, ~ 30 $km^2$) was measured throughout the study period; however, the surface inflow discharge to Loch Kinord and the small inflow discharge to Loch Davan were not measured. The agricultural land use in the Logie Burn catchment prevented the use of the measured discharge to estimate the natural inflows to Loch Kinord and Loch Davan. Discharge scaling has also previously been used within the upper Dee River catchment to estimate discharge in ungauged basins (Hrachowitz, Soulsby, Tetzlaff, & Speed, 2010; Wade, 1999). An evaluation of the discharge peak flow and timing in each of the three closest catchments (Bruntland Burn, Girnock Burn, and River Gairn) using the Engle-Granger cointegration test showed that each catchment can statistically described the flow and timing of the other catchments ($p$ = 1E−3 for all tests; Engle & Granger, 1987). The surrounding catchments also have a consistent annual rainfall-runoff ratio (0.58–0.65), which is well within the measurement uncertainty of precipitation and streamflow gauging (±5%; Scottish Environment Protection Agency (SEPA), 2018a). Additionally, the baseflow indices of the Girnock Burn and River Gairn (adjacent to the Dinnet Burn catchment) have little variability (0.464 and 0.452, respectively; SEPA, 2018b). This suggests that the surrounding region and adjacent catchments have similar catchment processes, and discharge scaling of the surrounding catchments may be suitable for ungauged streamflow into each lake. The unmeasured surface inflows of Loch Davan and Loch Kinord share similar catchment characteristics to the Bruntland Burn, including topology, geology, and temporal trends of measured isotopic compositions. Red Burn (secondary inflow) in Loch Davan and the inflow to Loch Kinord were therefore estimated by scaling the discharge of the Bruntland Burn using a ratio of catchment areas:

$$Q_{\text{in}} = Q_{\text{BB}} \cdot \left( \frac{\text{CA}_{\text{in}}}{\text{CA}_{\text{BB}}} \right) \tag{2}$$

where $Q_{\text{in}}$ is the estimated lake inflow, $Q_{\text{BB}}$ is the Bruntland Burn inflow, $\text{CA}_{\text{in}}$ is the catchment area of the lake inflow, and $\text{CA}_{\text{BB}}$ is the catchment area of the Bruntland Burn. The use of equation (2) with the Girnock Burn or River Gairn discharge each yield a root mean square error of 0.07 mm/day in comparison to the scaled Bruntland Burn discharge.

#### 4.1.2. Lake Evaporation

The potential evaporation was estimated using meteorological measurements from a meteorological station in the Bruntland Burn using the Penman equation (Penman, 1948). The vertical transport efficiency coefficient ($K_E$) was estimated using an empirical relationship to lake area ($K_E = (1.69 \cdot 10^{-5}) \cdot A^{-0.05}$; Harbek, 1962). Due to spatial differences of the measurement location and potential differences of meteorological measurements over vegetation at the Bruntland Burn relative to over lake water at Loch Kinord or Loch Davan, a calibration parameter ($\chi$, parameter range 0 to 2) was applied to the potential evaporation:

$$E_a = \chi \cdot E_P \tag{3}$$

where $E_a$ is the actual lake evaporation. The calibration parameter yields a simple scaled estimate of the Penman equation and maintains the temporal variability of evaporative flux.

#### 4.1.3. Lake Discharge

Lake discharge was estimated by closing the water balance (equation (1)). The water balance of each lake uses scaled estimates of surface inflow (equation (2)), measured inflow (Logie Burn, Loch Davan only), calibrated evaporation (equation (3)), and measured lake level from Loch Kinord. A simple linear relationship between discharge to lake depth was used to estimate the discharge:

$$Q = a \cdot D(t, V(t)) + b \tag{4}$$

where $a$ and $b$ are fitting parameters. More complex discharge-lake depth relationships were tested but did not yield significant improvements to closure of the water balance. For consistency, equation (4) was used for both lakes. In Loch Kinord, the parameters $a$ and $b$ in equation (4) were iteratively solved by minimizing the difference of simulated and measured lake depths using equation (1) ($\min(D(t, V(t)) - D_{\text{adj}})$ at all time steps). In the absence of lake depth for Loch Davan, the average and maximum lake level in Loch Davan ($\overline{D_L}$ and $\max(D_L)$, respectively) were assumed to be the same as the average and maximum measured lake level in Loch Kinord ($\overline{D_K}$ and $\max(D_K)$, respectively). For Loch Davan, the parameters $a$ and $b$ in equation (4) were iteratively solved by minimization of differences of the simulated average lake level to the assumed average lake

level ( $\min\left(\overline{|D(t,V(t))|} - \left|\overline{D_L}\right|\right)$ ), and the simulated maximum lake level and the assumed maximum lake level ($\min(\max(D(t,V(t))) - \max(D_L))$). The lake level and discharge for each lake were estimated daily using equations (1)–(4) in conjunction with the D-V-A relationships for each lake.

### 4.2. StorAge Selection Functions in Lakes

The concepts of storage-dependent transit time functions are well suited to characterize different catchment storages, including lakes, though the potential with regard to the latter has not yet been explored. The shallow depths and moderate temperature regime of Loch Kinord and Loch Dava suggest that the lakes likely do not result in permanent, uniform stratification. Furthermore, seasons have noticeably different inflow discharge and lake levels (Figure 2), which replicate the annual sinuosity of air and lake temperatures. Changes in lake transit time functions due to temperature and lake level are therefore related, and the time-variant transit time function may be described using a storage-dependent function.

The conceptualization of SAS functions is based on accounting for the age of each parcel of water in storage. This is accomplished by ranking water using the elapsed time it has spent in storage, termed the age-ranked storage ($S_T$). At any time ($t$), $S_T(T,t)$ represents the volume of water in storage that has an age that is younger than age $T$. The age-ranked storage changes in time with the addition of new water via precipitation and surface inflow, in conjunction with the outward fluxes of lake discharge and evaporation. Each flux is assigned a distribution (SAS function in cumulative distribution form, $\Omega$), which describes the quantity of water of age $T$ contributing to the flux. Inflow to storage is represented as a pulse; therefore, the SAS function for all inflow were negated (Harman, 2015). For both precipitation and surface inflow, the age of inflow is considered as new water to the lake and assigned an age of zero days. The new water contributions with age of zero days are used to define the beginning of the elapsed time water spends in storage prior to exiting via discharge or evaporation. For each lake, the governing equation of the conservation of mass of $S_T$ was described as follows:

$$\frac{\partial S_T(T,t)}{\partial t} = \mathrm{I}_1(t) + \mathrm{I}_2(\mathrm{t}) + P(t) - Q(t)\cdot\Omega_Q(S_T(T,t),t) - E(t)\cdot\Omega_E(S_T(T,t),t) - \frac{\partial S_T(T,t)}{\partial T} \tag{5}$$

The SAS functions were defined for lake discharge and evaporation fluxes using the uniform and gamma distributions. The uniform distribution provides an approximation of random sampling (complete mixing) of the volume leaving the lake. For very small lakes driven by wind advection this is likely the primary mixing regime. The uniform distribution SAS function of evaporation and discharge was assigned as follows:

$$\Omega_\varnothing(S_T,t) = \begin{cases} \dfrac{S_T}{S^u_\varnothing(t)} & S_T < S^u_\varnothing(t) \\ 1 & S_T > S^u_\varnothing(t) \end{cases} \tag{6}$$

where $\varnothing$ indicates the flux (evaporation or discharge) and $S^u_\varnothing(t)$ is a uniform distribution parameter. The distribution parameter is time variant and changes with the volume of water in the lake. While the uniform distribution can isolate specific water ages younger than $S^u_\varnothing(t)$ to leave storage, there is no preferential movement of water younger than $S^u_\varnothing(t)$. Preferential movement of water can also occur in small lakes and thereby influence the age of water flux. For this study, a gamma distribution was assumed to be representative of preferential water movement:

$$\Omega_\varnothing(S_T,t) = \frac{\gamma\left(\alpha, \frac{S_T}{S^g_\varnothing(t)}\right)}{\Gamma(\alpha)} \tag{7}$$

where $\alpha$ is a gamma distribution shape parameter, and $S^g_\varnothing(t)$ is a gamma distribution scale parameter. The variables, $S^u_\varnothing(t)$ and $S^g_\varnothing(t)$, used in equations (6) and (7) are time variant using lake volume:

$$S^*_\varnothing(t) = (\lambda\cdot N(V(t)) - \lambda\cdot\Delta Sc)^\beta \tag{8}$$

where * indicates the distribution ($u$ for uniform and $g$ for gamma), $\lambda$ is a linear slope parameter ($\lambda \neq 0$), $N(V(t))$ is normalized lake volume ($\frac{V-\overline{V}}{\sigma_V}$), $\Delta$Sc is an intercept parameter, and $\beta$ is a nonlinearity parameter. Similar to storage discharge parameters, the units of $\lambda$ change with $\beta$ to maintain dimensional consistency (Kirchner,

2009). The linear slope parameter ($\lambda$) describes how lake volumes influence the estimated mixing. Negative $\lambda$ decreases $S^*_{\varnothing}(t)$ and indicates an inverse storage effect (e.g., Harman, 2015), with an emphasized higher young water preference during high lake levels. Conversely, positive $\lambda$ increases $S^*_{\varnothing}(t)$ and indicates a direct storage effect and higher old water preference during high lake levels. High $\beta$ (>1) nonlinearly exaggerates the variability of $S^*_{\varnothing}$, while low values of $\beta$ ($0 \le \beta < 1$) nonlinearly dampens the variability of $S^*_{\varnothing}$. For each time step, $S_T$ was updated with lake inflows ($T = 0$), while the flux and lake water ages were estimated using the age balance (equation (5)) and SAS functions (equations (6)–(8), $\Omega_{\varnothing}(S_T, t)$). The mean age of lake discharge was defined as $\tau_T$, and the mean age of lake storage was defined as $\tau_R$.

### 4.3. StorAge Selection Isotope Mass Balance

#### 4.3.1. Lake Mass Balance

The isotope mass balance was resolved using the same water selection method as the age balance (equations (5)–(8)). For each water age, there is a corresponding isotopic composition of lake water ($\delta_L(S_T, t)$). To estimate the mass balance for all time steps, spline interpolation was used to gap-fill lake surface inflow isotopic compositions from biweekly or monthly, to daily. The isotopic inflow to the lake ($\delta_I$ and $\delta_P$, surface inflow and precipitation, respectively) was flux weighted to a single lake water composition for each time ($t$) $\left(\delta_L(0,t) = \left(\delta_P{\cdot}P + \delta_{I_{(1)}}{\cdot}I_{(1)} + \delta_{I_{(2)}}{\cdot}I_{(2)}\right)/\left(I_{(1)} + I_{(2)} + P\right)\right)$. The isotopic compositions of fluxes (discharge and evaporation) were estimated by integrating the contribution of water ages:

$$\delta_Q(t) = \int_0^S \omega_Q(S_T, t){\cdot}\delta_L\,(S_T, t){\cdot}\mathrm{d}S_T \tag{9}$$

where $\omega_Q(S_T, t)$ is the corresponding probability density function of $\Omega_Q(S_T, t$;i.e., $\Omega(S_T, t) = \int \omega(S_T, t) \cdot \mathrm{d}S_T)$.

#### 4.3.2. Evaporative Fractionation

Evaporative fractionation has a significant influence on the isotopic composition of lake water. However, since evaporation may not occur from water parcels of all ages (equations (6) and (7)), fractionation should be addressed independently for each water age $T$. The cumulative ranked storage ($S_T$) can be discretized into each age of $T$, the noncumulative ranked storage ($S_T' = \mathrm{d}S_T(T)/\mathrm{d}T$). For each $T$, the Craig-Gordon (CG) model was used to estimate the isotopic composition of evaporation vapor ($\delta_E$; Craig & Gordon, 1965):

$$\delta_E(T) = \frac{\frac{\delta_L\left(S_T'\right)}{\alpha^+} - h{\cdot}\delta_A - \varepsilon}{1 - \mathrm{h} + \frac{\varepsilon_K}{1{,}000}} \tag{10}$$

where $\alpha^+$ is the liquid-vapor fractionation (Horita & Wesolowski, 1994), $h$ is relative humidity, $\delta_A$ is the ambient atmospheric isotopic composition, and $\varepsilon$ is the sum of the equilibrium fractionation ($\varepsilon^+$) and kinetic fractionation ($\varepsilon_K$). Kinetic fractionation is a function of $h$, aerodynamic diffusion ($n$) and the ratio of molecular diffusion coefficients ($C_K$; $\varepsilon_K = n \cdot C_K \cdot (1 - h)$). For small lakes, $n = 0.5$ and $C_K = 28.5$ and 25.1 for $\delta^2$H and $\delta^{18}$O, respectively (Gat, 2010). The atmospheric isotopic composition, $\delta_A$ was assumed to be in equilibrium with the precipitation isotopic composition ($\delta_P$; Gibson et al., 2016). The mass balance for each time step and each $T$ (modified from Gibson, 2002):

$$S_T'{\cdot}\frac{\mathrm{d}\delta_L\left(S_T', t\right)}{\mathrm{d}t} + \delta_L\left(S_T', t\right){\cdot}\frac{\mathrm{d}S_T'}{\mathrm{d}t} = -Q(T){\cdot}\delta_L\left(S_T', t\right) - E(T){\cdot}\delta_E(T) \tag{11}$$

For a given time step ($t$), the fluxes ($Q$ and $E$) and $\delta_E$ do not change. Since $T = 0$ for lake inflow, for any $T > 0$ there is no additional inflow and the volume of age $T$ desiccates. The substitution of the CG model (equation (10)) into equation (11) yields an equation with one unknown ($\delta_L\left(S_T', t\right)$), which was solved similarly to the method shown in Gibson (2002) for each $T$ and $t$.

### 4.4. Long-Term Water Age Balance

To provide a first-order estimate of how lakes affect catchment transit times, a comparison of the transit time downstream of each lake was conducted, first using only lake discharge isotopes ($TTD_1$) and second using the convolution of lake inflow and lake transit times ($TTD_2$). The time-invariant gamma distribution with the convolution integral, corrected for evapotranspiration was used to estimate $TTD_1$ (McGuire & McDonnell, 2006). The estimation of $TTD_2$ required additional assessment of the transit times within the lake as well as the

transit times of surface water inflow to the lake. The transit times of the lake were estimated using the long-term average of the assumed SAS function, termed the marginal distribution ($MD_L$; Benettin et al., 2017; Heidbüchel et al., 2012). For the reason that there are potential similarities of the marginal distribution, to the time-invariant transit time in catchments without lakes (Benettin et al., 2015, 2017), we estimated the inflow ($TTD_{in}$) using the same method as $TTD_1$. Precipitation ($TTD_P$) was assigned as a pulse input with an input age of zero days, similar to the definition of precipitation age in equation (5). Weighted convolution of $TTD_{in}$, $MD_L$ and $TTD_P$ was used to estimate $TTD_2$:

$$TTD_2 = F_P \cdot \int_0^t (TTD_P(t) \cdot (MD_L(t))) \cdot dt + F_{in(1)} \cdot \int_0^t \left(TTD_{in(1)} \cdot (MD_L(t))\right) \cdot dt + F_{in(2)} \int_0^t \left(TTD_{in(2)}\ (MD_L(t))\right) \cdot dt \quad (12)$$

where $F_P$ is the fraction of precipitation to total lake inflow, $F_{in(1)}$ is the fraction of primary surface inflow to total lake inflow, and $F_{in(2)}$ is the fraction of secondary surface inflow to total lake inflow. The difference between $TTD_1$and $TTD_2$ shows the apparent influence of not accounting for lakes in the estimation of the catchment transit times.

### 4.5. Model Calibration

Dual isotope plots ($\delta^2H$ versus $\delta^{18}O$) help to visually distinguish different sources of water, detect general trends in mixing patterns relative to precipitation, and identify the influence of evaporation using deviations from the precipitation isotopic compositions. The coefficient of variability, the ratio of the standard deviation to the mean isotopic composition, may help to identify differences in isotopic variability and responsiveness of different water sources. The deviation from the precipitation compositions can be quantified using line-conditioned excess (lc-excess). The lc-excess is the Euclidian distance of a measured composition from the LMWL (Landwehr & Coplen, 2006):

$$lc - excess = \delta^2H - SL \cdot \delta^{18}O - INT \quad (13)$$

where SL is the slope and INT is the intercept of the LMWL. Negative values of lc-excess indicate evaporation enriched water. Using lc-excess helps to account for the large seasonal variability of precipitation, which may otherwise influence the evaporation line (Benettin et al., 2018). The differences of the mean lc-excess of lake inflow and outflow were tested for significance using two-tailed *t* tests (95% confidence).

Water balance parameters ($\chi$ and $B_E$) and SAS function parameters ($\alpha$, $\lambda$, and $\Delta Sc$ for evaporation and discharge) were calibrated simultaneously for the reason that the SAS functional form influences the evaporative fractionation in lake discharge. For example, high values of $B_E$ increase total lake evaporation and fractionation (high $B_E$ increases surface area), while the SAS function influences the evaporation and fractionation of each age $T$ (equations (6)–(8)). Therefore, $\chi$ estimated using measured isotopic composition of lake water is dependent on the total evaporation ($B_E$) and the SAS functional form (e.g., young water preferences).

The time variance of lake transit times was assessed using three SAS functional forms: (1) uniform distribution with linear dependence on storage ($\mathbf{U_L}$, $\beta = 1$), (2) gamma distribution with linear dependence on storage ($\mathbf{\Gamma_L}$, $\beta = 1$), and (3) gamma distribution with nonlinear dependence on storage ($\mathbf{\Gamma_\beta}$, $0 < \beta \leq 2$). The $\mathbf{U_L}$ SAS function is more parsimonious than $\mathbf{\Gamma_L}$ or $\mathbf{\Gamma_\beta}$ and is only dependent on the changes in storage. However, preferential mixing of water ages is likely in many lakes (Kalinin et al., 2016). The $\mathbf{\Gamma_L}$ SAS function considers both changes in storage and the preferential selection of different water ages ($\alpha$ shape parameter). Preferential mixing (gamma distribution) is likely for Loch Kinord and Loch Davan due to the close proximity of the inlet relative to the lake outlet in Loch Davan (Figure 1) and the very shallow lake levels near the lake shores (Loch Kinord and Loch Davan).

Calibration was conducted using 50,000 Monte Carlo simulations, retaining the 100 best simulations for analysis. Simulations were evaluated for all times greater than twice the theoretical hydraulic retention time (HRT = lake volume/lake inflow) to minimize the influence of initial conditions. The HRTs were 260 and 18 days for Loch Kinord and Loch Davan, respectively. Daily values of lake water level, and $\delta^2H$ and $\delta^{18}O$ in lake discharge were simulated for each lake from July 2014 to August 2016. Simulated lake discharge $\delta^2H$ and $\delta^{18}O$ using each SAS function were evaluated on days of measured lake discharge $\delta^2H$ and $\delta^{18}O$. Isotopic

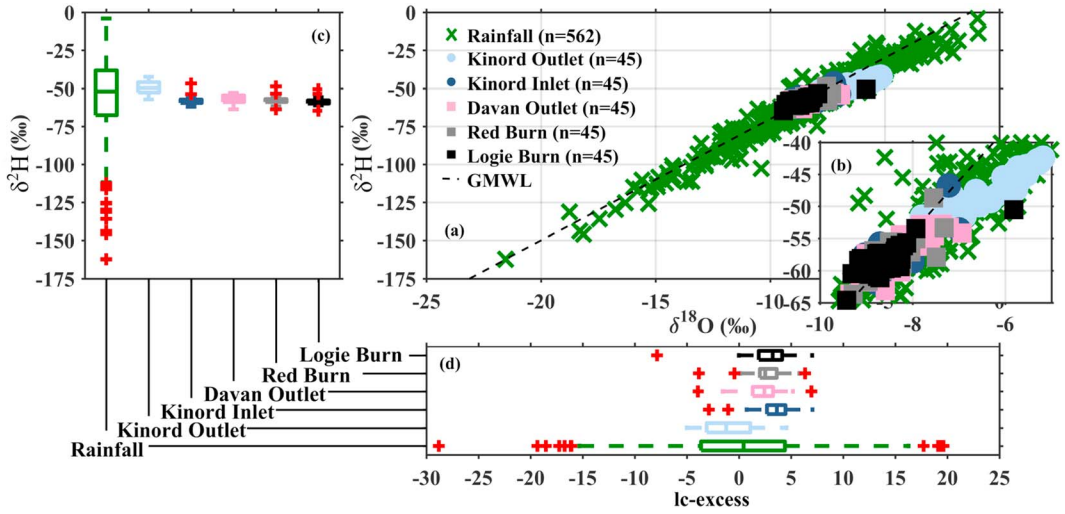


**Figure 3.** (a) Deuterium and oxygen-18 of lake inflows, outflows, and precipitation samples (*n* indicates number of samples and GWML is the Global Meteoric Water Line). The inset plot (b) focuses on the isotopic compositions of lake inflow and outflows. Boxplots of (c) deuterium and (d) line-conditioned excess are shown for all samples collected.

simulations were evaluated using the Nash-Sutcliffe (NSE, Nash & Sutcliffe, 1970) and Kling-Gupta (KGE, Kling et al., 2012) efficiencies. In Loch Kinord, the daily simulated lake level was evaluated against daily measured lake levels using the NSE and KGE. The efficiencies of NSE and KGE for $\delta^2$H and water level were used to calibrate the SAS functions and water balance. NSE was used to optimize the simulated $\delta^2$H for the large observed peak events (Figure 2c). KGE was used to optimize the simulated temporal variability of the isotopic compositions within the lakes. Simulations of $\delta^{18}$O were used as an additional objective function to validate the lake enrichment; however, they were not used to inform the 100 best simulations.

Due to the uncertainty of estimated inflow, the sensitivity of lake isotopic compositions was examined by varying the inflow discharge of the 100 best calibrated parameter sets. The inflow discharge (scaled discharge, equation (2)) was varied by attenuating the flow using the Muskingum-Cunge equation (Cunge, 1969). The Muskingum parameters were chosen ($k$ = 2 and $X$ = 0.1) to shift the discharge peaks by 1 day and maintain higher attenuated flows relative to the discharge used in calibration. These conditions were chosen to test potential variability of timing of large precipitation events as well as uncertainty in precipitation amounts. Temporal sensitivity on isotopic compositions of lake water was assessed using isotopic residuals:

$$R = \delta_s - \delta_{s,a} \tag{14}$$

where $R$ is the residual isotopic composition, $\delta_s$ is the simulated isotopic composition using area scaled discharge, and $\delta_{s,\,a}$ is the simulated isotopic compositions using area scaling with attenuation of discharge.

## 5. Results

### 5.1. Dynamics of Lake Inflow and Outflow Stable Isotope Compositions

The isotopic composition of precipitation had the highest annual variability of all sampled waters, increasing by 20‰ on average from winter (January) to summer (July) for $\delta^2$H (Figure 3). However, the isotopic composition of lake inflows had limited variability relative to precipitation and rarely deviated from the LMWL. Generally, inflows were most isotopically depleted during winter high flows and enriched during summer events. The isotopic compositions of outflows for both lakes were more variable than surface inflow (coefficient of variation, CV, Table 2), although this was not as visually apparent for Loch Davan (Figure 3). The slope of the linear regression of $\delta^2$H on $\delta^{18}$O for Loch Kinord was lower for outflow than either surface water inflow or precipitation, but for Loch Davan, the slope of the linear regression of $\delta^2$H on $\delta^{18}$O was higher for the lake outflow than the inflow (Table 2). However, the regression slope of the inflows had high uncertainty (±1.18)

**Table 2**
*Slopes and Intercepts of Linear Regression of $\delta^2H$ on $\delta^{18}O$ for Primary Inflows and Outflows of Loch Davan and Loch Kinord*

| Statistical Metrics of $\delta^2H$ and $\delta^{18}O$ | Red burn | Logie burn | Davan outlet | Kinord inlet | Kinord outlet | Rainfall |
|---|---|---|---|---|---|---|
| Slope | 4.51 | 4.03 | 4.54 | 4.61 | 4.43 | 7.62 |
| Intercept | −19.83 | −23.82 | −19.57 | −18.44 | −19.91 | 3.85 |
| $R^2$ | 0.55 | 0.53 | 0.71 | 0.62 | 0.93 | 0.94 |
| CV ($\sigma/\mu$) | 0.032 (0.039) | 0.041 (0.046) | 0.050 (0.067) | 0.043 (0.049) | 0.086 (0.141) | 0.434 (0.418) |

*Note.* Also shown is the slope and intercept of the linear regression of the local meteoric water line (rainfall), and the regression statistics for each inflow and outflow.

and low coefficients of determination ($R^2$ = 0.55 and 0.53, Table 2). With the exception of Loch Kinord outflow, lake surface inflows and outflows were significantly more depleted for average $\delta^2H$ and had higher average lc-excess than the mean of precipitation (95% confidence, Figures 3c and 3d). These two conditions were most consistent with the isotopic composition of winter precipitation.

The lc-excess of lake surface inflow was less temporally variable than precipitation (flux-weighted values in Figure 4). The lc-excess of lake outflow for both lakes decreased sharply during June to October prior to an increase between November to March. Loch Kinord outflow lc-excess was continuously lower during the winter months than the inflow; however, this was not observed for Loch Davan. The evaporative effects within Loch Kinord resulted in significantly different mean lc-excess of the inflow relative to the outflow ($p \ll 0.001$). In Loch Davan, the mean outlet lc-excess was significantly different from the Logie Burn inflow ($p$ = 0.01); however, it was not statistically different to the smaller inflow (Red Burn), which was influenced by evaporation from wetlands ($p$ = 0.13). The lc-excess rapidly increased in both lakes during the extreme precipitation event from the end of December 2015 to the beginning of January 2016.

### 5.2. Lake Water Balance and Modeling

Reasonable model fits to water level (Loch Kinord) and the isotopic composition of lake outflows were obtained for each SAS function with NSE and KGE values ranging from 0.70 to 0.97 (Table 3). For Loch Kinord, the NSE and KGE of $\delta^2H$ simulations were the best with the $\mathbf{\Gamma_L}$ and $\mathbf{\Gamma_\beta}$ SAS functions; however, the distinction between linear ($\mathbf{\Gamma_L}$) and nonlinear ($\mathbf{\Gamma_\beta}$) dependence on storage for preferential mixing was not evident (Table 3). The $\mathbf{U_L}$ SAS function in Loch Davan had the best model efficiency ($\delta^2H$), most notably for KGE. Similar to Loch Kinord, there was little difference between the linear ($\mathbf{\Gamma_L}$) and nonlinear ($\mathbf{\Gamma_\beta}$) dependence on storage for the preferential mixing functional forms.

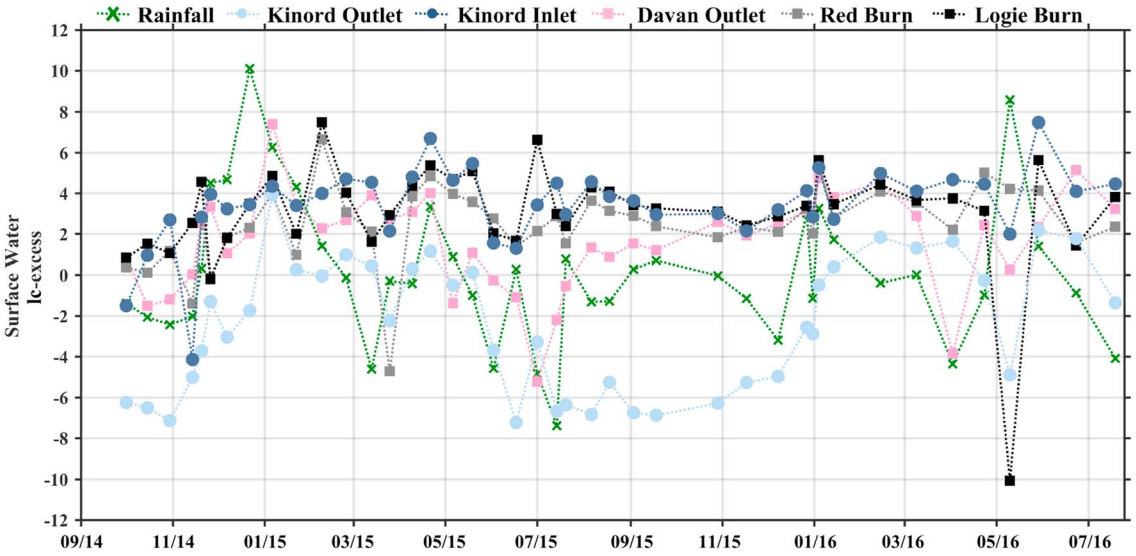


**Figure 4.** Time series of line-conditioned excess (lc-excess) for the surface inflow and outflow of Loch Kinord (circles) and Loch Davan (squares). Additionally shown is the observed precipitation lc-excess (green cross), shown as flux-weighted values on the lake sample days.

**Table 3**
*Efficiency Criteria of the Best Performance for Each Model*

| | | | |
|---|---|---|---|
| Uniform linear storage-dependent distribution model ($U_L$) | | | |
| Lake | NSE: $\delta^2$H (NSE: $\delta^{18}$O) | KGE: $\delta^2$H (KGE: $\delta^{18}$O) | NSE Lake Level |
| Kinord | 0.88(0.86) | 0.88(0.82) | 0.89 |
| Davan | 0.73(0.70) | 0.88(0.85) | N/A |
| Gamma linear storage-dependent distribution model ($\Gamma_L$) | | | |
| Lake | NSE: $\delta^2$H (NSE: $\delta^{18}$O) | KGE: $\delta^2$H (KGE: $\delta^{18}$O) | NSE |
| Kinord | 0.93(0.87) | 0.97(0.86) | 0.89 |
| Davan | 0.70(0.69) | 0.79(0.76) | N/A |
| Gamma nonlinear storage-dependent distribution model ($\Gamma_\beta$) | | | |
| Lake | NSE: $\delta^2$H (NSE: $\delta^{18}$O) | KGE: $\delta^2$H (KGE: $\delta^{18}$O) | NSE |
| Kinord | 0.91(0.88) | 0.95(0.92) | 0.89 |
| Davan | 0.72(0.69) | 0.79(0.77) | N/A |

*Note*. Where applicable, the Nash-Sutcliffe (NSE) and Kling-Gupta (KGE) of the simulated isotopic composition of $\delta^2$H, $\delta^{18}$O, and water level are shown. No statistical fit was applicable for Loch Davan as water level was not measured. N/A = not applicable.

The sign of the calibrated $\lambda$ in the SAS function for each lake defines the distinction between a direct storage effect and inverse storage effect. For discharge from Loch Kinord, $\mathbf{U_L}$ showed an inverse storage effect and $\mathbf{\Gamma_L}$ and $\mathbf{\Gamma_\beta}$ showed direct storage effects, while evaporation showed direct storage effects for all SAS functions (Figure 5a). For Loch Kinord, the identifiability of $\lambda$ ($p(\lambda_Q)$ and $p(\lambda_E)$) was similar for both discharge and evaporation using the $\mathbf{\Gamma_L}$ and $\mathbf{\Gamma_\beta}$ SAS functions. The estimated storage effects in Loch Davan were inverse storage effects for discharge and direct storage effects for evaporation and were consistent for all SAS functions. The shape parameter ($\alpha$) was substantially different for both evaporation and discharge in each lake than the typically observed value in catchment flow systems (~0.5). For Loch Kinord, $\beta_Q$ had the highest occurrence near one, which resulted in a linear dependence on storage for $\mathbf{\Gamma_\beta}$. The difference of $\mathbf{\Gamma_L}$ and $\mathbf{\Gamma_\beta}$ SAS functions in Loch Davan was more pronounced, with the highest occurrence of $\beta_Q < 1$ indicating nonlinear damping of the storage variability. In each lake, $\beta_E$ had the highest occurrence $>1$, which increased the influence of storage variability on the SAS function. However, $\beta_E$ had the highest variability for each lake. The parameters, $\Delta$Sc and $B_E$ were insensitive for all discharge and evaporation SAS function forms.

### 5.3. Evaluation of Lake Isotope Simulations

The simulated isotope compositions captured the annual variability of those measured in the outflow of each lake (Figure 6). Each SAS function reproduced the ~10‰ annual variability of $\delta^2$H in Loch Davan relative to the larger ~15‰ annual variability of $\delta^2$H in Loch Kinord. The SAS functions also simulated the dynamics of isotopic enrichment due to evaporation and the isotopic response to the large precipitation event in December 2015/January 2016 for both lakes. However, the uncertainty in simulated $\delta^2$H in Loch Davan was much larger during the event and the SAS functions were unable to capture the isotopic composition in Loch Kinord during late summer 2016 and October 2014 in Loch Davan. The simulated $\delta^2$H was consistently enriched relative to the measured $\delta^2$H during the periods the SAS functions were unable reproduce measured compositions. The difference between $\mathbf{U_L}$ and $\mathbf{\Gamma_L}$ and $\mathbf{\Gamma_\beta}$ SAS functions was apparent in the simulated summer isotopic variability and lake water fractionation (Figure 6). The daily variability of $\delta^2$H with the $\mathbf{U_L}$ SAS function was more damped than the $\mathbf{\Gamma_L}$ or $\mathbf{\Gamma_\beta}$ SAS functions. In Loch Kinord, direct storage effects of the $\mathbf{\Gamma_L}$ and $\mathbf{\Gamma_\beta}$ SAS functions resulted in suppression of the isotopic composition of large inflows. The inverse storage effect in Loch Davan resulted in a large increase in lake isotopic composition toward the new precipitation composition. The $\mathbf{U_L}$ SAS function resulted in periodic overenrichment during the summer months in Loch Davan and during the winter months in Loch Kinord, which was not observed with the $\mathbf{\Gamma_L}$ or $\mathbf{\Gamma_\beta}$ SAS functions. The lake isotopic composition was most sensitive to changes in inflow discharge (equation (14)) during the peak flow event in December 2015/January 2016 (Figures 6b and 6d). The sensitivity of inflow discharge on lake compositions was the greatest in Loch Kinord for the $\mathbf{U_L}$ SAS function. Loch Davan composition was more sensitive relative to Loch Kinord (±10‰), while the $\mathbf{\Gamma_L}$ SAS function was most sensitive to changes in discharge.

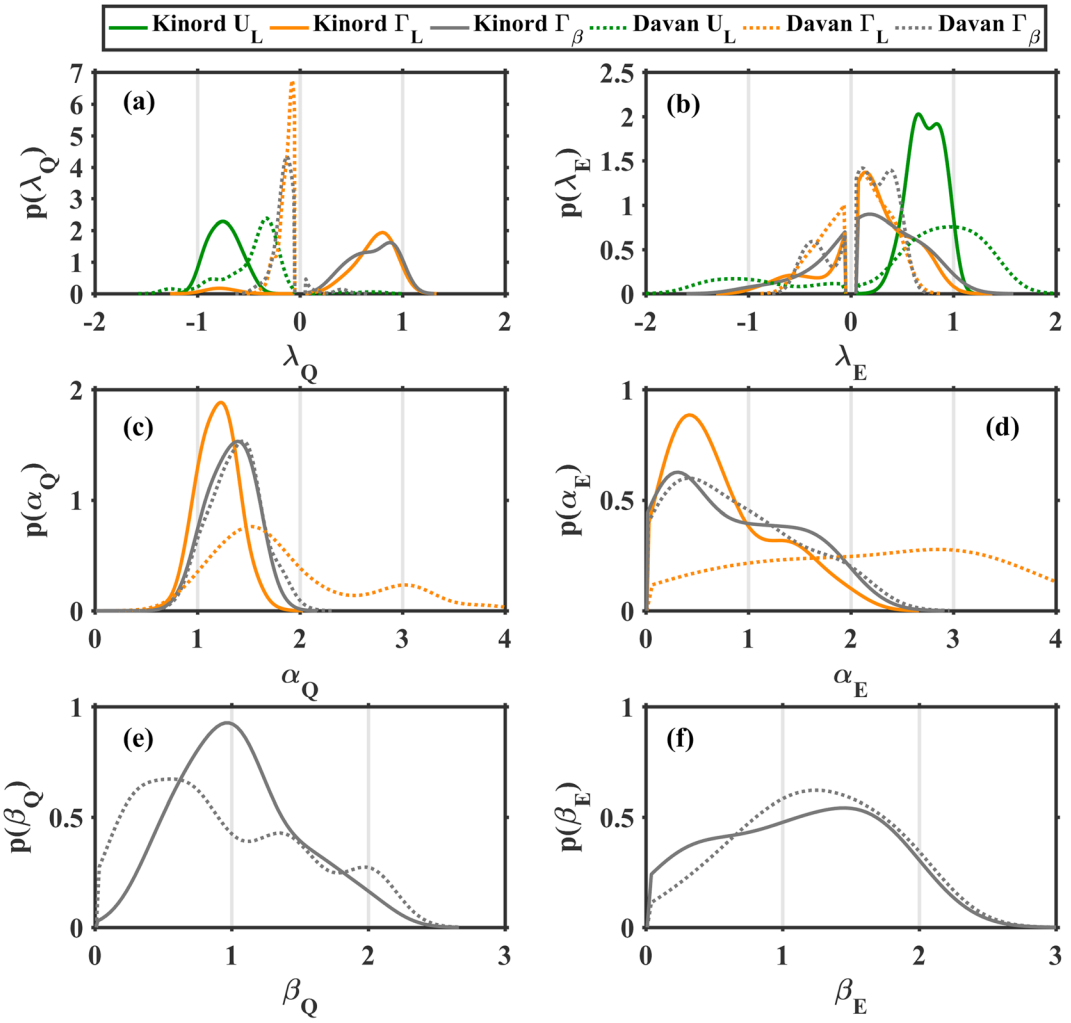


**Figure 5.** Parameter probability distributions for the most sensitive transit time parameters (a) $\lambda_Q$, (b) $\lambda_E$, (c) $\alpha_Q$, (d) $\alpha_E$, (e) $\beta_Q$, and (f) $\beta_E$. Values of $\lambda$ (discharge and evaporation) were either positive or negative ($\lambda \neq 0$). Parameters used in uniform distribution with linear dependence on storage ($U_L$) are shown in green, gamma distribution with linear dependence on storage ($\Gamma_L$) are shown in orange, and gamma distribution with nonlinear dependence on storage ($\Gamma_\beta$) are shown in gray. Loch Kinord is shown with solid lines and Loch Davan is shown with dotted lines.

In Loch Kinord, simulation confidence bounds did not vary greatly throughout the year, typically ranging between ±1–2.5‰ in $\delta^2$H for the $\mathbf{\Gamma_L}$ and $\mathbf{\Gamma_\beta}$ SAS functions and ±0.5–1‰ in $\delta^2$H for the $\mathbf{U_L}$ SAS function (Figure 6a). The largest confidence bounds for isotopic compositions coincided with the largest precipitation events. Unlike Loch Kinord, the width of the confidence bounds for $\delta^2$H simulations in Lock Davan was temporally variable, being greatest during the summer and the December 2015/January 2016 event. With the exception of the December 2015/January 2016 event, the inverse storage effect in Loch Davan resulted in lower uncertainty on average in $\delta^2$H during winter (±0.25‰) and higher uncertainty in $\delta^2$H during the summer (±1‰) due to evaporation fractionation for all SAS functions. For each lake, the simulation of $\delta^{18}$O (not shown) was relatively similar, the isotopic uncertainties were proportionally smaller and did not provide substantially different information (Table 3).

### 5.4. Estimated Lake Evaporation

The estimated evaporation rate ($\chi$ calibration parameter) changed with each SAS function (Figures 7a and 7d). Through calibration, the parameter range of $\chi$ decreased to 0.43 to 1.0, for all SAS functions and both lakes. In both lakes, the calculated average annual evaporation was greatest for the $\mathbf{\Gamma_\beta}$ SAS function

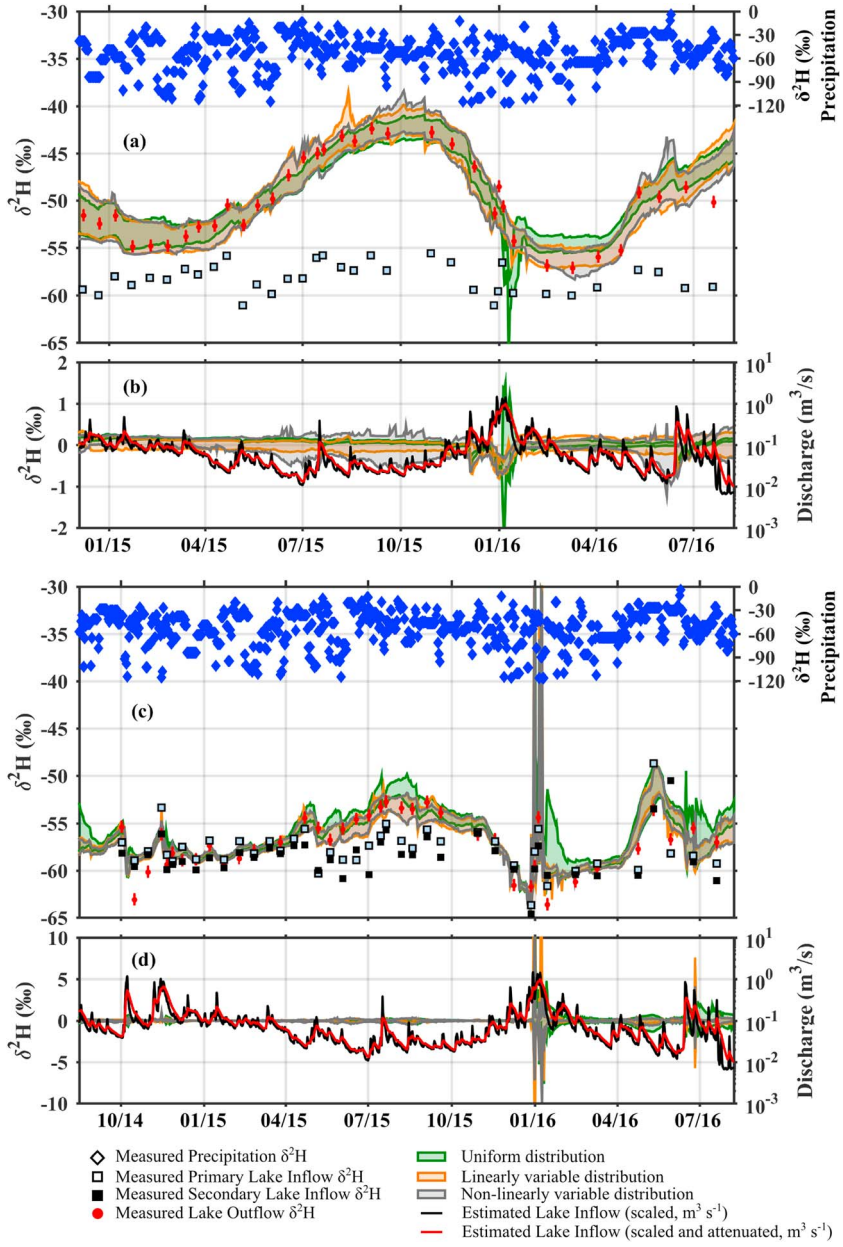


**Figure 6.** Simulated $\delta^2$H for (a) Loch Kinord and (c) Loch Davan for each model. The 95% confidence bounds are shown for the uniform distribution with linear dependence on storage ($U_L$, green), gamma distribution with linear dependence on storage ($\Gamma_L$, orange), and gamma distribution with nonlinear dependence on storage ($\Gamma_\beta$, gray) models, with the isotopic measurements and analytical uncertainty bounds. The sensitivity of lake isotopic compositions to discharge for each model are shown for (b) Loch Kinord and (d) Loch Davan.

(407 and 438 mm/year for Loch Kinord and Loch Davan, respectively). Conversely, the $\mathbf{U_L}$ SAS function resulted in the lowest average annual evaporation for both lakes (342 and 401 mm/year for Loch Kinord and Loch Davan, respectively). Unlike the evaporation rate, the ratio of evaporation to inflow (E/I) incorporates the estimation of lake surface area due to differences in the elevation correction parameter ($B_E$). The ratio E/I was very small for both lakes (<0.15). In both lakes E/I increased with the number of model parameters ($\mathbf{U_L} > \mathbf{\Gamma_L} > \mathbf{\Gamma_\beta}$; Figures 7b and 7e). The increase in E/I coincided with greater evaporation uncertainty and younger estimated evaporation ages (Figures 7c and 7f). While the uncertainty of evaporation flux was greater for the $\mathbf{\Gamma_L}$ and $\mathbf{\Gamma_\beta}$ SAS functions, the uncertainty of the simulated isotopic compositions was not proportionally larger.

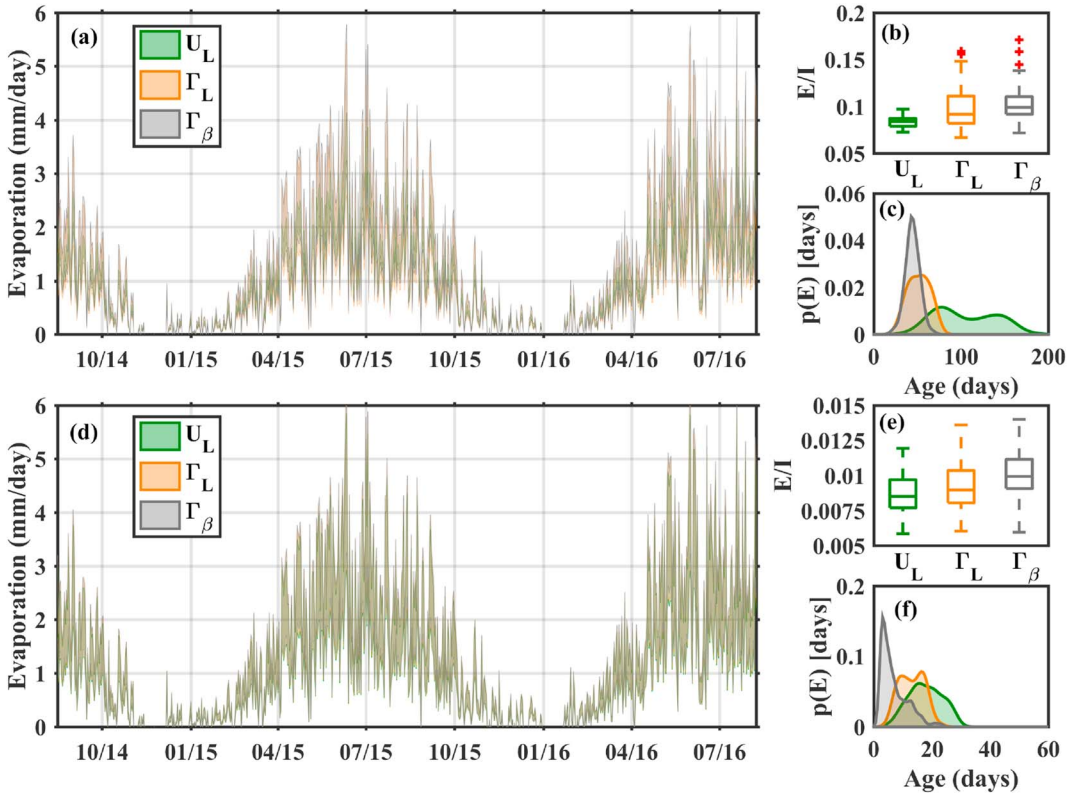


**Figure 7.** Estimated daily lake evaporation (mm/day), the ratio of evaporation to inflow (*E/I*), and the probability distribution of mean daily evaporation age for Loch Kinord (a–c) and Loch Davan (d–f). Wider uncertainty bounds of $\Gamma_L$ and $\Gamma_\beta$ resulted in orange and gray appearance of the evaporation bounds (a and d).

The estimated age of evaporation changed with each SAS function, with a wider distribution of mean annual evaporation ages for $\mathbf{U_L}$ than $\mathbf{\Gamma_L}$ and $\mathbf{\Gamma_\beta}$ (Figures 7c and 7f). In Loch Kinord, the direct storage effect for evaporation resulted in relatively constant evaporation age during the summer, with minor fluctuations due to summer precipitation events. The shape of the distribution of mean modeled evaporation age was similar to a normal distribution for each SAS function (Figure 7c), with distribution median values of 99 ($\mathbf{U_L}$), 50 ($\mathbf{\Gamma_L}$), and 43 ($\mathbf{\Gamma_\beta}$) days. In Loch Davan, the estimated mean daily evaporation age was young, and the SAS functions frequently selected water that was just a few days old. Evaporation age was youngest during the summer due to the calibrated direct storage effect. The median of the distribution of mean evaporation ages reflected the differences in each distribution: 17 ($\mathbf{U_L}$), 13 ($\mathbf{\Gamma_L}$), and 5 ($\mathbf{\Gamma_\beta}$) days. However, uncertainty of the evaporation age increased during the winter (high water level and low evaporation rate). This was likely due to lower influence of evaporation on the isotopic composition during the "flushing period," which was dominated by younger water (inverse storage for discharge effect).

### 5.5. Temporally Variable Lake Transit and Residence Times

The width of the 95% confidence bounds of the mean age of lake discharge in Loch Kinord ($\tau_T$, bands in Figure 8a) generally remained constant after July 2015 for the $\mathbf{U_L}$ and $\mathbf{\Gamma_L}$ SAS functions. The $\mathbf{\Gamma_\beta}$ SAS function resulted in more temporal variability in the $\tau_T$ confidence bounds throughout the simulation. The inverse storage effect with the $\mathbf{U_L}$ SAS function resulted in much younger estimated $\tau_T$ during the December 2015/January 2016 event and smaller variability of $\tau_T$ confidence bounds during the summer months than the $\mathbf{\Gamma_L}$ and $\mathbf{\Gamma_\beta}$ SAS functions. The mean lake discharge age was more sensitive to inflows for the direct storage effect ($\mathbf{\Gamma_L}$ and $\mathbf{\Gamma_\beta}$ SAS functions) than the inverse storage effect ($\mathbf{U_L}$ SAS function, Figure 8a, summer 2015 and 2016). In Loch Davan, all SAS functions resulted in high intra-annual variability of $\tau_T$ confidence bounds (Figure 8b). The confidence bounds were generally greatest during the drier summer months in 2015 and smallest during the large events in January 2016 and June 2016. The differences of the $\tau_T$ confidence

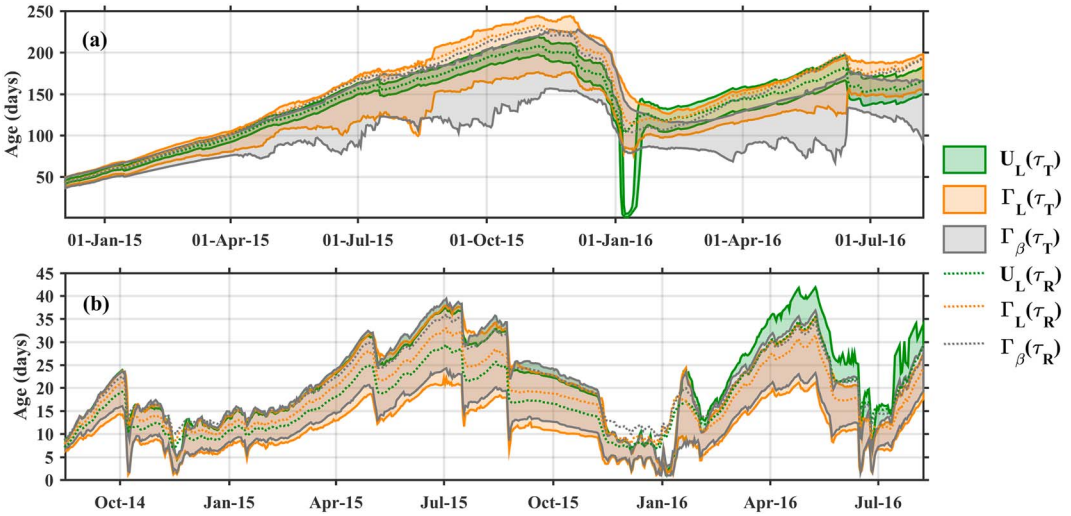


**Figure 8.** The 95% confidence intervals of the mean lake transit time (a) Loch Kinord and (b) Loch Davan are shown with shaded regions, while the average of the mean residence times are shown as a dotted line.

bounds with regard to the SAS functions were not clearly present for Loch Davan, possibly due to the short $\tau_T$. In both lakes, the higher preference of younger water to exit via discharge or evaporation resulted in an older mean lake residence time ($\tau_R$) than $\tau_T$ for the $\mathbf{\Gamma_L}$ and $\mathbf{\Gamma_\beta}$ SAS functions (Figure 8). Conversely, $\tau_R$ for the $\mathbf{U_L}$ SAS function in each lake was most consistent with the mean $\tau_T$ during the low flow periods and only showed distinctly higher $\tau_R$ than $\tau_T$ during the peak event in January 2016.

### 5.6. Influence of Evaporation and Lake Transit Time Estimations at the Catchment Scale

The mean of $TTD_1$ ($MTT_1$) for each lake was noticeably lower than the mean of $TTD_{in}$ (Table 4). The lower $MTT_1$ coincides with a higher coefficient of variation, CV, in lake outflow relative to the inflow. However, the decrease of $MTT_1$ from inflow to outflow was not directly proportional to the change of CV from inflow to outflow (Table 2). With respect to Loch Davan, Loch Kinord had a smaller difference between the mean of $TTD_{in}$ and $MTT_1$, relative to the difference of CV for inflow and CV for lake outflow. The CV was consistently larger for $\delta^{18}O$ than $\delta^2H$ and had a noticeably greater difference at the outflow of each lake. Despite the moderate transit time of Loch Kinord the mean of the convolution of $TTD_{in}$ and lake marginal distribution ($MD_L$) resulted in a mean age of $TTD_2$ younger than the mean of $TTD_{in}$. This is likely due to the proportion of precipitation ($F_P$), which contributes water of age zero days (Table 4). In Loch Davan, the uncertainty of the mean of $TTD_2$ was relatively similar to the lake transit time, which shows an insignificant effect of the lake to change the inflow water ages prior to the lake outflow. Unlike in Loch Kinord, the low proportion of precipitation on Loch Davan

**Table 4**
*The Mean Marginal Age of Fluxes, Ratios of Inflow and Outflow Fluxes, and the Mean of the Marginal Age of the Catchment Downstream of Each Lake (Loch Kinord and Loch Davan)*

| | Loch Kinord | | | Loch Davan | | |
|---|---|---|---|---|---|---|
| Inflow and Outflow Transit Times | Outflow convolution | | | | | |
| Primary inflow (mean of $TTD_{in(1)}$, years) | 2.82 ± 0.47 | | | 2.51 ± 0.41 | | |
| Secondary inflow (mean of $TTD_{in(2)}$, years) | N/A | | | 3.14 ± 0.15 | | |
| Catchment downstream of the lake (mean of $TTD_1$, years) | 1.35 ± 0.19 | | | 1.92 ± 0.34 | | |
| | Inflow and lake transit time convolution | | | | | |
| | $U_L$ | $\Gamma_L$ | $\Gamma_\beta$ | $U_L$ | $\Gamma_L$ | $\Gamma_\beta$ |
| Mean of the marginal distribution of lake discharge ($MD_L$, days) | 122.8 ± 6.6 | 135.7 ± 10.9 | 121.7 ± 11.3 | 11.5 ± 1.9 | 11.0 ± 2.0 | 11.6 ± 1.8 |
| Mean of the inflow and lake convolution ($TTD_2$, years) | 2.18 ± 0.11 | 2.12 ± 0.10 | 2.15 ± 0.12 | 2.52 ± 0.04 | 2.52 ± 0.04 | 2.52 ± 0.04 |
| Primary inflow to iotal Inflow ratio ($F_{in(1)} = I_{in(1)}/I_T$) | 0.74 ± 0.02 | 0.71 ± 0.02 | 0.73 ± 0.02 | 0.83 ± 0.01 | 0.83 ± 0.01 | 0.83 ± 0.01 |
| Precipitation to Total Inflow ratio ($F_P = P/I_T$) | 0.26 ± 0.02 | 0.29 ± 0.02 | 0.27 ± 0.02 | 0.024 ± 0.01 | 0.025 ± 0.01 | 0.026 ± 0.01 |

($F_P < 3\%$, Table 4) resulted in no noticeable change in lake outflow water age. For both lakes, the transit time estimated using the convolution of inflow and lake transit time ($TTD_2$) was significantly older than the transit time estimated using only the lake outflow ($TTD_1$, 99% confidence).

## 6. Discussion

### 6.1. What Are the Implications of Lakes for Catchment Isotopic Dynamics and Transit Time Analysis?

Lakes mix and attenuate the isotopic composition of surface water inflow and precipitation and are thus an important component of hydrological systems that need to be appropriately conceptualized in catchment travel time studies. However, this issue has received little attention to date. Catchment transit time distributions have traditionally been assessed using lumped models, though tracer-aided modeling studies have similarly shown the importance of separating the influence of lake effects on stream water isotopic compositions (Birkel et al., 2011a). For catchment transit times downstream of a lake, the separation of the lake transit time from the lake inflow transit time was shown here to be essential for the isolation of evaporation fractionation and precipitation effects on the lake from the transport effect in both the catchment and lake. The decrease of lc-excess in the outflows of each lake relative to their inflows (Figure 3d) indicates evaporative fractionation within the lakes. The consistently negative lc-excess during low evaporation periods in Loch Kinord potentially indicates a memory effect from evaporation in the previous summer, whereas the annual convergence of lc-excess during winter in Loch Davan indicate shorter residence times (Figure 4). The differences in the coefficient of variation of $\delta^2H$ and $\delta^{18}O$ of inflows and outflows are possible simple indicators of the relative effects of mixing and evaporation. The magnitude of the increase in the CV from lake inflow to lake outflow may yield a simple indicator of the effect of evaporation, with a larger increase in CV indicating greater evaporation fractionation influence (Table 4). With the previously established relationships correlating MTT to the variability of measured tracers, the lack of consideration of lakes in catchment transit time will lead to the danger of overestimating mixing and a lower derived MTT (Godsey et al., 2010).

Confounding the obvious expectation that the transit time of lakes will increase overall catchment transit times, direct precipitation and evaporation have a potential influence on the mean catchment water age downstream of lakes (Table 4). Precipitation, evaporation, and lake transit time simultaneously influence water age and isotopic variability. Precipitation decreases mean catchment transit time and increases isotopic variability, while lake transit time increases mean catchment transit time and decreases isotopic variability. Evaporation, while not explicit in equation (12), increases the mean transit time through the lake and increases isotopic variability of the lake outflow. As the mean of $MD_L$ increases, the relative difference of $TTD_{in}$ and $TTD_p$ with respect to $MD_L$ decreases and $TTD_2$ is more dependent on $MD_L$ ($MD_L + TTD_{in} \cong MD_L + TTD_P$). In catchments or events where the lake is predominantly fed by precipitation ($F_P \rightarrow 1$) and has a low mean of $MD_L$, the catchment outflow would be mostly event water. In lake systems with a more balanced precipitation relative to surface water inflow (i.e., Loch Kinord) and low $MD_L$ relative to inflow transit time, this may result in a reduction of the mean catchment transit time due to the contribution of young precipitation on the lake.

### 6.2. How Do the Flux-Dependent SAS Functions Inform on Lake Mixing?

The capacity of SAS functions to inform on lake mixing is dependent on how well the model captures the observed dynamics as well as the uncertainty associated with model simulations. There are notable periods in the simulations of Loch Davan which are overenriched in $\delta^2H$ while providing reasonable lc-excess simulations. However, the uncertainty of simulated lake isotopes likely does not influence the estimation of $\lambda$ since there are few such occurrences. A direct comparison of the lake inflow isotopic composition to the Bruntland Burn streamflow isotopic composition suggests that the overestimation in Loch Davan may instead reflect an occasional effect of the relatively coarse fortnightly sampling of inflow. Although high uncertainty of $\delta^2H$ in Loch Davan outflow occurs during the one high storage event in January 2016 (equating to >100-year return period), the uncertainty is associated primarily with the large volume of new water "flushed" as a pulse by the SAS function rather than uncertainty in storage effect ($\lambda_Q$). The pulse of new water leaving the lake during a short period is on occasion overly influenced by evaporation. Lastly, any potential uncertainty of the altitude effect of precipitation (section 3) is likely minimal as the long-term uncertainty is well within the model confidence bounds for both lakes.

The consistency of calibrated parameters suggest that Loch Kinord undergoes direct storage effects for discharge and evaporation, while Loch Davan undergoes inverse storage effects for discharge and direct storage effects for evaporation. These trends are the most consistent for the preferential mixing SAS functions (gamma distribution). These storage effects and mixing assumptions ($\mathbf{\Gamma_L}$ and $\mathbf{\Gamma_\beta}$ SAS functions) correlate well to the physical processes within each lake while reproducing the most appropriate isotopic dynamics, such as limited overfractionation. With the consideration of physically appropriate mixing estimation and reasonable isotope enrichment relative to the $\mathbf{U_L}$ SAS function, the lake water mixing in Loch Kinord and Loch Davan is likely best represented by the gamma distribution. The identification of the likelihood of the storage effect during high (or low) water can help to constrain the parameterization of the SAS function. Near surface mixing may be influenced by a number of conditions, including vegetation (in the lake margins or on the lake bed, e.g., Figure 9b), limiting the mixing of newer water (Herb & Stefan, 2004; Sharip et al., 2012), rapid flow paths (e.g., Figure 9a) of the primary stream inflows to the outlet (Englert & Stewart, 1983), and thermal stratification (e.g., Figures 9c and 9) resulting in only mixing of new water in the upper layers (e.g., Kalinin et al., 2016).

In Loch Kinord, low lake storage reduces mixing of the lake and results in younger water near the surface, which is consistent with some stratification of warmer incoming water relative to deeper lake water (e.g., precipitation dominated, Figure 9c). In other shallow lakes, low water level may expose significant shoreline vegetation (Figure 9b), which may hinder both horizontal (Herb & Stefan, 2004) and vertical mixing (Rueda et al., 2006). The limited horizontal mixing due to vegetation reduces the effective lake mixing volume during summer, thereby increasing the probability for younger surface water to leave via the lake outlet. While a lake may be affected by both vegetation and stratification, the distinction of dominant processes may be apparent with the evaporation storage effect (Figure 9b versus Figure 9c). Limited vertical mixing in vegetation-affected lakes (e.g., Figure 9b) may result in older water near the surface for evaporation and more uniform selection of evaporation age. However, a stratified lake (e.g., Figure 9c) may depict younger evaporated water since the younger epilimnion water may not mix well with the older hypolimnion water (Castellano et al., 2010; Pilotti et al., 2014). Furthermore, if stratification was substantial then the actual lake residence time should be longer than the HRT (Ambrosetti et al., 2003). The opposite storage effect of discharge and evaporation in Loch Davan indicated considerably different flow patterns. The relatively close proximity of the largest inflow (Logie Burn) to the outlet suggests natural short circuiting of the lake (Figure 9a) during high storage periods (Englert & Stewart, 1983). The small lake area and the high proportion of surface inflow to total lake volume likely result in the higher proportion of younger water near the surface (young evaporation age).

Generally, it can be anticipated that many catchments show inverse storage effects, with newer water bypassing storage during high antecedent storage conditions (Benettin et al., 2017; Birkel et al., 2012; Harman, 2015; Hrachowitz et al., 2013; van der Velde et al., 2012; van Huijgevoort et al., 2016). However, lakes likely have additional factors influencing the storage effect including the following: wind, stratification, groundwater upwelling, surface water flows, and internal waves (Spigel & Imberger, 1987). The use of storage selection for both discharge and evaporation can help for initial identification of lake mixing processes (Figure 9). For example, the evaporation storage effect for both lakes in this study, combined with the low lake storage during the summer, suggests that summer surface water inflows and precipitation preferentially remained near the lake surface and may have some limited vertical mixing within the lake. In highly seasonal northern lakes, stratification is the most significant control on the mixing (Gibson, 2002). During the summer months when evaporation is dominant, the presence of newer water near the surface is dependent on the temperature of the inflow (Martin & McCutcheon, 1999) and the heat capacity of the lake (Carmack, 1979). Under the conditions that inflow temperatures are similar to the temperature at the lake surface, newer water may remain near the surface, readily evaporating and results in a lower discharge transit time (Kalinin et al., 2016; Waugh et al., 2002). This would suggest either direct storage for both discharge and evaporation (Figure 9c), or inverse storage for both fluxes (Figure 9d), dependent on the summer lake storage relative to winter. The framework presented here can be used to test this hypothesis with $\delta^2$H and $\delta^{18}$O lakes with an HRT less than around 5 years, which is generally accepted as the limit of determining isotopic outputs from inputs in MTT studies (McGuire & McDonnell, 2006). Applications of SAS functions may be further applied to lakes with a larger surface area or deeper bathymetry by introducing temperature and spatial scales into the SAS functions. For example, a circular shallow lake may have fewer rapid flow paths if the surface inflow

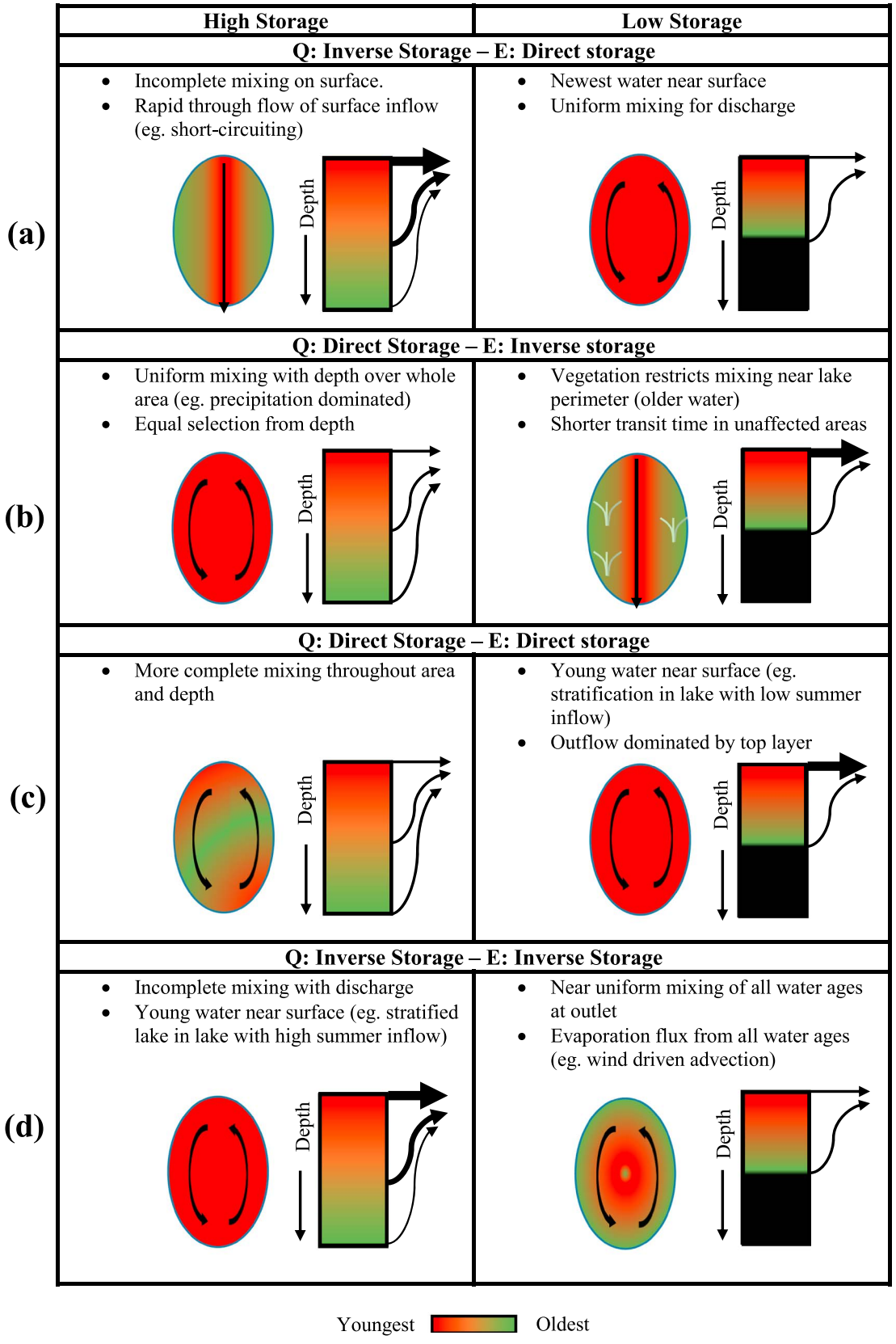


**Figure 9.** Lake mixing patterns shown with plan view (oval) and depth (rectangle) against the estimated water age. The plan view shows the age of water available for evaporation and width of arrows indicates the preference of discharge from depth. Depth is the age-ranked accumulation of water.

further rather than closer to the outlet. Accounting for spatial distances in larger lakes could result in different mixing patterns of precipitation and surface water inflows. However, in deeper and highly seasonal lakes, the thermal stratification is the key control on how inflow is affected by lake water mixing and therefore influences the probability of water selection for discharge or evaporation (Ambrosetti et al., 2003; Piontelli & Tonolli, 1964; Rossi et al., 1975).

The lake residence times and the age of outflows and evaporation flux affect the biogeochemistry and ecology of lakes. In general, the evaporation estimated for the study lakes was similar to open water evaporation reported for other nearby Scottish lakes of 6–7 mm/day during the summer (Tyler et al., 2007). Some of the differences between the peak summer evaporation rates may be due to the measurement of meteorological conditions over land rather than over water as well as the use of stable isotopic compositions to calibrate the evaporation with different mixing assumptions using SAS functions. While the values of $\chi$ were lower than expected (0.43–1.0), this is likely due to the assumption of negligible heat storage within shallow lakes. In some small lakes, heat storage may result in the overestimation of evaporation when using the Penman equation and assumed negligible heat storage (Finch & Hall, 2001; McCuen & Asmussen, 1973). The overestimation effects are primarily restricted to the summer months and it is anticipated that $\chi$ was low to reduce the summer evaporation from the lakes. The *E*/*I* ratio has been shown to be positively correlated to carbon and nutrient loadings (Brooks et al., 2014; Jeppesen et al., 2011; Yuan et al., 2011), while residence time generally is negatively correlated to lake nutrient levels (Brooks et al., 2014; Cardille et al., 2007; Hanson et al., 2003). In lakes with direct storage effects for discharge and inverse storage effects for evaporation, the lake may simultaneously experience temporal increases in *E*/*I* and decreases in residence time, compounding an increase in anticipated lake nutrient levels. Furthermore, the lakes were shown to have different seasonal trends in residence time (Figure 8), which may help explain seasonal changes in lake nutrients (Romo et al., 2013). Clearly, the use of lake travel time analysis has great potential for informing biogeochemical studies seeking to understand the dynamics of nutrients and other pollutants.

## 7. Conclusions

Our study extended the use of SAS functions to lake-influenced systems to identify the effect of the temporal variability of lake discharge and evaporation flux ages on catchment transit times. The use of uniform mixing and preferential mixing assumptions were related to storage in two lake-influenced catchments using mass balance of water and stable water isotopes ($\delta^2$H and $\delta^{18}$O). The use of SAS functions allowed us to identify temporal dynamics of the ages of both lake discharge and evaporation. During low lake level periods in the summer, evaporation preferentially selected young water. The dynamics of lake outflow selection with time were different for each lake; the large lake selected the youngest water during low lake storage periods, while the small lake selected the youngest water during the high lake storage periods. These differences are driven by both the size difference of each lake and the spatial location of the lake inflows and can be explained with the SAS framework presented here. Furthermore, testing of the catchment-scale approach of TTD estimation against a disaggregation of upstream and lake influence on the catchment TTD revealed the sensitivity of transit times to lake evaporation effects.

Time-variant transit time functions have a wide applicability to catchment scale and subcatchment-scale water age estimation as they simplify the physical mixing mechanisms into a statistical similar physical representation. This study has shown successful application for lake-influenced catchments and provides a general framework for constraining lake mixing processes identified by SAS functions. Further potential application of SAS functions within lakes could explore the use of probabilistic selections using water temperatures for stratification and possible spatial disaggregation of surface inflow sources at the outlet.

**Acknowledgments**
We would like to thank the European Research Council (ERC, project GA 335910 VeWa) for funding the project and the Rural Environment Science and Analytical Services Division of the Scottish Government for funding collection of surface discharge measurements. Jonathan Dick and Josie Geris are kindly acknowledged for running the isotope analysis. The authors thank Bernhard Scheliga and Hannah Braun for occasional isotopic sample collection, the Scottish Environmental Protection Agency for water level data, and Stephen Addy, Carol Taylor, and Helen Watson (James Hutton Institute) for discharge gauging and maintenance. The authors thank the reviewers for their valuable feedback during the review. The data used are available on the University of Aberdeen PURE data repository (doi: 10.20392/6ea64264-4db1-4e7d-826a-168cf4295c3f).

## References

Ala-aho, P., Soulsby, C., Wang, H., & Tetzlaff, D. (2017). Integrated surface-subsurface model to investigate the role of groundwater in headwater catchment runoff generation: A minimalist approach to parameterisation. *Journal of Hydrology*, *547*, 664–677. https://doi.org/10.1016/j.jhydrol.2017.02.023

Ambrosetti, W., Barbanti, L., & Sala, N. (2003). Residence time and physical processes in lakes. *Journal of Limnology*, *62*(1s), 1–15. https://doi.org/10.4081/jlimnol.2003.s1.1

Ameli, A. A., & Creed, I. F. (2017). Quantifying hydrologic connectivity of wetlands to surface water systems. *Hydrology and Earth System Sciences*, *21*(3), 1791–1808. https://doi.org/10.5194/hess-21-1791-2017

Anderson, M. P., & Cheng, X. (1993). Long- and short-term transience in a groundwater/lake system in Wisconsin, USA. *Journal of Hydrology*, *145*(1–2), 1–18. https://doi.org/10.1016/0022-1694(93)90217-W

Asano, Y., Uchida, T., & Ohte, N. (2002). Residence times and flow paths of water in steep unchannelled catchments, Tanakami, Japan. *Journal of Hydrology*, *261*(1–4), 173–192. https://doi.org/10.1016/S0022-1694(02)00005-7

Benettin, P., Kirchner, J. W., Rinaldo, A., & Botter, G. (2015). Modeling chloride transport using travel time distributions at Plynlimon, Wales. *Water Resources Research*, *51*, 3259–3276. https://doi.org/10.1002/2014WR016600

Benettin, P., Soulsby, C., Birkel, C., Tetzlaff, D., Botter, G., & Rinaldo, A. (2017). Using SAS functions and high-resolution isotope data to unravel travel time distributions in headwater catchments. *Water Resources Research*, *53*(3), 1864–1878. https://doi.org/10.1002/2016WR020117

Benettin, P., Volkmann, T. H. M., von Freyberg, J., Frentress, J., Penna, D., Dawson, T. E., & Kirchner, J. W. (2018). Effects of climatic seasonality on the isotopic composition of evaporating soil waters. *Hydrology and Earth System Sciences Discussions*, 1–16. https://doi.org/10.5194/hess-2018-40

Birkel, C., Geris, J., Molina, M. J., Mendez, C., Arce, R., Dick, J., et al. (2016). Hydroclimatic controls on non-stationary stream water ages in humid tropical catchments. *Journal of Hydrology*, *542*, 231–240. https://doi.org/10.1016/j.jhydrol.2016.09.006

Birkel, C., Soulsby, C., Tetzlaff, D., Dunn, S., & Spezia, L. (2012). High-frequency storm event isotope sampling reveals time-variant transit time distributions and influence of diurnal cycles. *Hydrological Processes*, *26*(2), 308–316. https://doi.org/10.1002/hyp.8210

Birkel, C., Tetzlaff, D., Dunn, S. M., & Soulsby, C. (2011a). Using lumped conceptual rainfall-runoff models to simulate daily isotope variability with fractionation in a nested mesoscale catchment. *Advances in Water Resources*, *34*(3), 383–394. https://doi.org/10.1016/j.advwatres.2010.12.006

Birkel, C., Tetzlaff, D., Dunn, S. M., & Soulsby, C. (2011b). Using time domain and geographic source tracers to conceptualize streamflow generation processes in lumped rainfall-runoff models. *Water Resources Research*, *47*, W02515. https://doi.org/10.1029/2010WR009547

Botter, G. (2012). Catchment mixing processes and travel time distributions. *Water Resources Research*, *48*, W05545. https://doi.org/10.1029/2011WR011160

Botter, G., Bertuzzo, E., & Rinaldo, A. (2010). Transport in the hydrologic response: Travel time distributions, soil moisture dynamics, and the old water paradox. *Water Resources Research*, *46*, W03514. https://doi.org/10.1029/2009WR008371

Botter, G., Bertuzzo, E., & Rinaldo, A. (2011). Catchment residence and travel time distributions: The master equation. *Geophysical Research Letters*, *38*, L11403. https://doi.org/10.1029/2011GL047666

Brooks, J. R., Gibson, J. J., Birks, S. J., Weber, M. H., Rodecap, K. D., & Stoddard, J. L. (2014). Stable isotope estimates of evaporation: Inflow and water residence time for lakes across the United States as a tool for national lake water quality assessments. *Limnology and Oceanography*, *59*(6), 2150–2165. https://doi.org/10.4319/lo.2014.59.6.2150

Cardille, J. A., Carpenter, S. R., Coe, M. T., Foley, J. A., Hanson, P. C., Turner, M. G., & Vano, J. A. (2007). Carbon and water cycling in lake-rich landscape connections, lake hydrology, and biogeochemistry. *Journal of Geophysical Research*, *112*, G02031. https://doi.org/10.1029/2006JG000200

Carmack, E. C. (1979). Combined influence of inflow and Lake temperatures on spring circulation in a riverine Lake. *Journal of Physical Oceanography*, *9*(2), 422–434. https://doi.org/10.1175/1520-0485(1979)009<0422:CIOIAL>2.0.CO;2

Castellano, L., Ambrosetti, W., Barbanti, L., & Rolla, A. (2010). The residence time of the water in Lago Maggiore (N. Italy): First results from an Eulerian-Lagrangian approach. *Journal of Limnology*, *69*(1), 2. https://doi.org/10.3274/JL10-69-1-02

CEH (2017). Center for Ecology and Hydrology UK Lakes Portal. Retrieved from https://eip.ceh.ac.uk/apps/lakes/detail.html#wbid=21123, (Accessed 1 January 2017)

Craig, H., & Gordon, L. I. (1965). Deuterium and oxygen 18 variations in the ocean and marine atmosphere. In E. Tongiogi (Ed.), *Proc. Stable Isotopes in Oceanographic Studies and Paleotemperatures* (pp. 9–130). Spoleto, Italy: V. Lishi e F., Pisa.

Cunge, J. A. (1969). On the subject of a flood propagation computation method (Muskingum method). *Journal of Hydraulic Research*, *7*, 205–230.

Edwards, K. J. (1979). Palynological and temporal inference in the context of prehistory, with special reference to the evidence from lake and peat deposits. *Journal of Archaeological Science*, *6*(3), 255–270. https://doi.org/10.1016/0305-4403(79)90003-7

Engle, R. F., & Granger, C. W. J. (1987). Co-integration and error-correction: Representation, estimation, and testing. *Econometrica*, *55*(2), 251–276. https://doi.org/10.2307/1913236

Englert, J. P., & Stewart, K. M. (1983). Natural short-circuiting of inflow to outflow through Silver Lake, New York. *Water Resources Research*, *19*(2), 529–537. https://doi.org/10.1029/WR019i002p00529

Finch, J. W., & Hall R. L. (2001). Estimation of open water evaporation: A review of methods, Environment Agency R&D Technical Report W6–043/TR

Froehlich, K. F. O., Gonfiantini, R., & Rozanski, K. (2005). Isotopes in lakes studies: A historical perspective. *Isotopes in the Water Cycle*, *381*. https://doi.org/10.1007/1-4020-3023-1_11

Gat, J. (1995). Stable isotopes of fresh and saline lakes. In *Physics and chemistry of lakes*, (pp. 139–165). Berlin Heidelberg New York: Spring-Verlag.

Gat, J. (2010). *Isotope hydrology: A study of the water cycle*. London: Imperial College Press.

Gibson, J. J. (2002). Short-term evaporation and water budget comparisons in shallow Arctic lakes using non-steady isotope mass balance. *Journal of Hydrology*, *264*(1–4), 242–261. https://doi.org/10.1016/S0022-1694(02)00091-4

Gibson, J. J., Birks, S. J., & Yi, Y. (2016). Stable isotope mass balance of lakes: A contemporary perspective. *Quaternary Science Reviews*, *131*, 316–328. https://doi.org/10.1016/j.quascirev.2015.04.013

Gibson, J. J., & Edwards, T. W. D. (1996). Development and validation of an isotopic method for estimating lake evaporation. *Hydrological Processes*, *10*(10), 1369–1382. https://doi.org/10.1002/(SICI)1099-1085(199610)10:10<1369::AID-HYP467>3.0.CO;2-J

Gibson, J. J., Edwards, T. W. D., & Bursey, G. G. (1993). Estimating evaporation using stable isotopes: Quantitative results and sensitivity analysis for two catchments in northern Canada. *Nordic Hydrology*, *24*(2–3), 79–94. https://doi.org/10.2166/nh.1993.006

Godsey, S. E., Aas, W., Clair, T. A., de Wit, H. A., Fernandez, I. J., Kahl, J. S., et al. (2010). Generality of fractal 1/f scaling in catchment tracer time series, and its implications for catchment travel time distributions. *Hydrological Processes*, *24*(12), 1660–1671. https://doi.org/10.1002/hyp.7677

Hanson, P. C., Bade, D. L., Carpenter, S. R., & Kratz, T. K. (2003). Lake metabolism: Relationships with dissolved organic carbon and phosphorus. *Limnology and Oceanography*, *48*(3), 1112–1119. https://doi.org/10.4319/lo.2003.48.3.1112

Harbek, G. E. (1962). A practical field technique for measuring reservoir evaporation utilizing mass-transfer theory, U.S. Geol. Surv. Prof. Pap., 272–E.

Harman, C. J. (2015). Time-variable transit time distributions and transport: Theory and application to storage-dependent transport of chloride in a watershed. *Water Resources Research*, *51*, 1–30. https://doi.org/10.1002/2014WR015707

Heidbüchel, I., Troch, P. A., & Lyon, S. W. (2013). Separating physical and meteorological controls of variable transit times in zero-order catchments. *Water Resources Research*, *49*, 7644–7657. https://doi.org/10.1002/2012WR013149

Heidbüchel, I., Troch, P. A., Lyon, S. W., & Weiler, M. (2012). The master transit time distribution of variable flow systems. *Water Resources Research*, *48*, W06520. https://doi.org/10.1029/2011WR011293

Herb, W. R., & Stefan, H. G. (2004). Temperature stratification and mixing dynamics in a shallow Lake with submersed Macrophytes. *Lake and Reservoir Management*, *20*(4), 296–308. https://doi.org/10.1080/07438140409354159

Horita, J., & Wesolowski, D. J. (1994). Liquid-vapor fractionation of oxygen and hydrogen isotopes of water from the freezing to the critical temperature. *Geochimica et Cosmochimica Acta*, *58*(16), 3425–3437. https://doi.org/10.1016/0016-7037(94)90096-5

Hrachowitz, M., Bohte, R., Mul, M. L., Bogaard, T. A., Savenije, H. H. G., & Uhlenbrook, S. (2011). On the value of combined event runoff and tracer analysis to improve understanding of catchment functioning in a data-scarce semi-arid area. *Hydrology and Earth System Sciences*, *15*(6), 2007–2024. https://doi.org/10.5194/hess-15-2007-2011

Hrachowitz, M., Savenije, H., Bogaard, T. A., Tetzlaff, D., & Soulsby, C. (2013). What can flux tracking teach us about water age distribution patterns and their temporal dynamics? *Hydrology and Earth System Sciences*, *17*(2), 533–564. https://doi.org/10.5194/hess-17-533-2013

Hrachowitz, M., Soulsby, C., Tetzlaff, D., Malcolm, I. A., & Schoups, G. (2010). Gamma distribution models for transit time estimation in catchments: Physical interpretation of parameters and implications for time-variant transit time assessment. *Water Resources Research*, *46*, W10536. https://doi.org/10.1029/2010WR009148

Hrachowitz, M., Soulsby, C., Tetzlaff, D., & Speed, M. (2010). Catchment transit times and landscape controls—Does scale matter? *Hydrological Processes*, *24*(1), 117–125. https://doi.org/10.1002/hyp.7510

Hughes, M., Hornby, D. D., Bennion, H., Kernan, M., Hilton, J., Phillips, G., & Thomas, R. (2003). The development of a GIS-based inventory of standing waters in Great Britain together with a rick-based prioritisation protocal. *Water, Air, and Soil Pollution*, *4*, 73–84.

Jeppesen, E., Kronvang, B., Olesen, J. E., Audet, J., Søndergaard, M., Hoffmann, C. C., et al. (2011). Climate change effects on nitrogen loading from cultivated catchments in Europe: Implications for nitrogen retention, ecological state of lakes and adaptation. *Hydrobiologia*, *663*(1), 1–21. https://doi.org/10.1007/s10750-010-0547-6

Kalinin, A., Covino, T., & McGlynn, B. (2016). The influence of an in-network lake on the timing, form, and magnitude of downstream dissolved organic carbon and nutrient flux. *Water Resources Research*, *51*, 1333–1352. https://doi.org/10.1002/2014WR015716

Kim, M., Pangle, L. A., Cardoso, C., Lora, M., Volkmann, T. H. M., Wang, Y., et al. (2016). Transit time distributions and StorAge Selection functions in a sloping soil lysimeter with time-varying flow paths: Direct observation of internal and external transport variability. *Water Resources Research*, *52*, 7105–7129. https://doi.org/10.1002/2016WR018620

Kirchner, J. W. (2009). Catchments as simple dynamical systems: Catchment characterization, rainfall-runoff modeling, and doing hydrology backward. *Water Resources Research*, *45*, W02429. https://doi.org/10.1029/2008WR006912

Kirchner, J. W., Feng, X., & Neal, C. (2001). Catchment-scale advection and dispersion as a mechanism for fractal scaling in stream tracer concentrations. *Journal of Hydrology*, *254*(1–4), 82–101. https://doi.org/10.1016/S0022-1694(01)00487-5

Kling, H., Fuchs, M., & Paulin, M. (2012). Runoff conditions in the upper Danube basin under an ensemble of climate change scenarios. *Journal of Hydrology*, *424-425*, 264–277. https://doi.org/10.1016/j.jhydrol.2012.01.011

Landwehr, J. M., & Coplen, T. B. (2006). Line-conditioned excess: A new method for characterizing stable hydrogen and oxygen isotope ratios in hydrologic systems, in International Conference on Isotopes in Environmental Studies – Aquatic Forum 2004, pp. 98–99.

Laudon, H., Spence, C., Buttle, J., Carey, S., McDonnell, J., McNamara, J., et al. (2017). Save norther high-latitude catchments. *Nature Geoscience*, *10*(5), 324–325. https://doi.org/10.1038/ngeo2947

Maloszewski, P., Rauert, W., Trimborn, P., Herrmann, A., & Rau, R. (1992). Isotope hydrological study of mean transit times in an alpine basin (Wimbachtal, Germany). *Journal of Hydrology*, *140*(1–4), 343–360. https://doi.org/10.1016/0022-1694(92)90247-S

Marsh, T. J., Kirby, C., Muchan, K. G. L., Barker, L. J., Henderson, E., & Hannaford, J. (2016). The winter floods of 2015/2016 in the UK—A review.

Martin, J. L., & McCutcheon, S. C. (1999). *Hydrodynamics and transport for water quality modeling*. Boca Raton, Fla: Lewis Publishers.

McCuen, R., & Asmussen, L. E. (1973). Estimating the effects of heat storage on evaporation rates. *Hydrological Sciences Journal*, *18*(2), 191–196. https://doi.org/10.1080/02626667309494026

McGuire, K. J., & McDonnell, J. J. (2006). A review and evaluation of catchment transit time modeling. *Journal of Hydrology*, *330*(3–4), 543–563. https://doi.org/10.1016/j.jhydrol.2006.04.020

Messager, M. L., Lehner, B., Grill, G., Nedeva, I., & Schmitt, O. (2016). Estimating the volume and age of water stored in global lakes using a geo-statistical approach. *Nature Communications*, *7*, 13,603. https://doi.org/10.1038/ncomms13603

Muñoz-Villers, L. E., Geissert, D. R., Holwerda, F., & McDonnell, J. J. (2016). Factors influencing stream baseflow transit times in tropical montane watersheds. *Hydrology and Earth System Sciences*, *20*(4), 1621–1635. https://doi.org/10.5194/hess-20-1621-2016

Nash, J. E., & Sutcliffe, J. V. (1970). River flow forecasting through conceptual models part I—A discussion of principles*. *Journal of Hydrology*, *10*(3), 282–290. https://doi.org/10.1016/0022-1694(70)90255-6

NLS, N. L. of S. (2017). Bathymetrical survey of the fresh-water lochs of Scotland, 1897–1909. Retrieved from http://maps.nls.uk/bathymetric/loch_order.html (Accessed 1 January 2017)

Penman, H. L. (1948). Natural evaporation from open water, bare soil and grass. *Proceedings of the Royal Society of London A*, *193*, 120–145. https://doi.org/10.1098/rspa.1948.0037

Pangle, L. A., Kim, M., Cardoso, C., Lora, M., Meira Neto, A. A., Volkmann, T. H. M., et al. (2017). The mechanistic basis for storage-dependent age distributions of water discharged from an experimental hillslope. *Water Resources Research*, *53*, 2733–2754. https://doi.org/10.1002/2016WR019901

Pilotti, M., Simoncelli, S., & Valerio, G. (2014). A simple approach to the evaluation of the actual water renewal time of natural stratified lakes. *Water Resources Research*, *51*, 4840–4847. https://doi.org/10.1002/2015WR017273

Piontelli, R., & Tonolli, V. (1964). Il tempo di residenza delle acque lacustri in relazione ai fenomeni di arricchimento in sostanze immesse, con particolare riguardo al Lago Maggiore. *Memorie dell'Istituto Italiano di Idrobiologia*, *17*, 247–266.

Queloz, P., Carraro, L., Benettin, P., Botter, G., Rinaldo, A., & Bertuzzo, E. (2015). Transport of fluorobenzoate tracers in a vegetated hydrologic control volume: 2. Theoretical inferences and modeling. *Water Resources Research*, *51*, 2793–2806. https://doi.org/10.1002/2014WR016508

Rinaldo, A., Benettin, P., Harman, C., Hrachowitz, M., McGuire, K., van der Velde, Y., et al. (2015). Storage selection functions: A coherent framework for quantifying how catchments store and release water and solutes. *Water Resources Research*, *51*, 4840–4847. https://doi.org/10.1002/2015WR017273

Rodgers, P., Soulsby, C., Waldron, S., & Tetzlaff, D. (2005). Using stable isotope tracers to identify hydrological flow paths, residence times and landscape controls in a mesoscale catchment. *Hydrology and Earth System Sciences Discussions*, *2*(1), 1–35. https://doi.org/10.5194/hessd-2-1-2005

Romo, S., Soria, J., Fernandez, F., Ouahid, Y., & Baron-Sola, Á. (2013). Water residence time and the dynamics of toxic cyanobacteria. *Freshwater Biology*, *58*(3), 513–522. https://doi.org/10.1111/j.1365-2427.2012.02734.x

Rossi, G., Ardente, V., Beonio-Brocchieri, F., & Diana, E. (1975). On the calculation of the mean residence time in monomictic lakes. *Hydrological Sciences Bulletin*, *20*(4), 575–580. https://doi.org/10.1080/02626667509491588

Rueda, F., Moreno-Ostos, E., & Armengol, J. (2006). The residence time of river water in reservoirs. *Ecological Modelling*, *191*(2), 260–274. https://doi.org/10.1016/j.ecolmodel.2005.04.030

Scottish Environment Protection Agency (SEPA) (2018a). SEPA rainfall data for Scotland. Retrieved from http://apps.sepa.org.uk/rainfall (Accessed 1 January 2018)

Scottish Environment Protection Agency (SEPA) (2018b). SEPA water level data. Retrieved from http://apps.sepa.org.uk/waterlevels/ (Accessed 1 January 2017)

Sharip, Z., Hipsey, M. R., Schooler, S. S., & Hobbs, R. J. (2012). Physical circulation and spatial exchange dynamics in a shallow floodplain wetland. *The International Journal of Design & Nature and Ecodynamics*, *7*(3), 274–291. https://doi.org/10.2495/DNE-V7-N3-274-291

Siegenthaler, U., & Oeschger, H. (1980). Correlation of $\delta^{18}O$ in precipitation with temperature and altitude. *Nature*, *285*(5763), 314–317. https://doi.org/10.1038/285314a0

Smart, R. P., Soulsby, C., Neal, C., Wade, A., Cresser, M. S., Billett, M. F., et al. (1998). Factors regulating the spatial and temporal distribution of solute concentrations in a major river system in NE Scotland. *Science of the Total Environment*, *221*(2–3), 93–110. https://doi.org/10.1016/S0048-9697(98)00196-X

Soulsby, C., Birkel, C., Geris, J., Dick, J., Tunaley, C., & Tetzlaff, D. (2015). Stream water age distributions controlled by storage dynamics and nonlinear hydrologic connectivity: Modeling with high-resolution isotope data. *Water Resources Research*, *51*, 7759–7776. https://doi.org/10.1002/2015WR017888

Soulsby, C., Birkel, C., Geris, J., & Tetzlaff, D. (2015). The isotope hydrology of a large river system regulated for hydropower. *River Research and Applications*, *31*, 335–349. https://doi.org/10.1002/rra

Soulsby, C., Dick, J., Scheliga, B., & Tetzlaff, D. (2017). Taming the flood—How far can we go with trees? *Hydrological Processes*, *31*(17), 3122–3126. https://doi.org/10.1002/HYP.11226

Soulsby, C., Malcolm, R., Gibbins, C., & Dilks, C. (2001). Seasonality, water quality trends and biological responses in four streams in the Cairngorm Mountains, Scotland, Hydrol. *Earth System Science*, *5*(3), 433–450. https://doi.org/10.5194/hess-5-433-2001

Soulsby, C., Malcolm, R., Helliwell, R., Ferrier, R. C., & Jenkins, A. (2000). Isotope hydrology of the Allt a' Mharcaidh catchment, Cairngorms, Scotland: Implications for hydrological pathways and residence times. *Hydrological Processes*, *14*(4), 747–762. https://doi.org/10.1002/(SICI)1099-1085(200003)14:4<747::AID-HYP970>3.0.CO;2-0

Soulsby, C., & Tetzlaff, D. (2008). Towards simple approaches for mean residence time estimation in ungauged basins using tracers and soil distributions. *Journal of Hydrology*, *363*(1–4), 60–74. https://doi.org/10.1016/j.jhydrol.2008.10.001

Speed, M., Tetzlaff, D., Hrachowitz, M., & Soulsby, C. (2011). Evolution of the spatial and temporal characteristics of the isotope hydrology of a montane river basin. *Hydrological Sciences Journal*, *56*(3), 426–442. https://doi.org/10.1080/02626667.2011.561208

Spigel, R. H., & Imberger, J. (1987). Mixing processes relevant to phytoplankton dynamics in lakes. *New Zealand Journal of Marine and Freshwater Research*, *21*(3), 361–377. https://doi.org/10.1080/00288330.1987.9516233

Tetzlaff, D., Birkel, C., Dick, J., Geris, J., & Soulsby, C. (2014). Storage dynamics in hydropedological units control hillslope connectivity, runoff generation, and the evolution of catchment transit time distributions. *Water Resources Research*, *50*(2), 969–985. https://doi.org/10.1002/2013WR014147

Tyler, J. J., Leng, M. J., & Arrowsmith, C. (2007). Seasonality and the isotope hydrology of Lochnagar, a Scottish mountain lake: Implications for palaeoclimate research. *The Holocene*, *17*(6), 717–727. https://doi.org/10.1177/0959683607080513

van der Velde, Y., Heidbüchel, I., Lyon, S. W., Nyberg, L., Rodhe, A., Bishop, K., & Troch, P. A. (2015). Consequences of mixing assumptions for time-variable travel time distributions. *Hydrological Processes*, *29*(16), 3460–3474. https://doi.org/10.1002/hyp.10372

van der Velde, Y., Torfs, P. J. J. F., van der Zee, S. E. A. T. M., & Uijlenhoet, R. (2012). Quantifying catchment-scale mixing and its effect on time-varying travel time distributions. *Water Resources Research*, *48*, W06536. https://doi.org/10.1029/2011WR011310

van Huijgevoort, M. H. J., Tetzlaff, D., Sutanudjaja, E. H., & Soulsby, C. (2016). Using high resolution tracer data to constrain water storage, flux and age estimates in a spatially distributed rainfall-runoff model. *Hydrological Processes*, *30*(25), 4761–4778. https://doi.org/10.1002/hyp.10902

Wade, A. (1999). Assessmet and modelling of water chemistry in a large catchment, River Dee, NE Scotland. Ph.D. dissertation. University of Aberdeen.

Waugh, D. W., Vollmer, M. K., Weiss, R. F., Haine, T. W. N., & Hall, T. M. (2002). Transit time distributions in Lake Issyk-Kul. *Geophysical Research Letters*, *29*(24), 2231. https://doi.org/10.1029/2002GL016201

Yuan, F., Sheng, Y., Yao, T., Fan, C., Li, J., Zhao, H., & Lei, Y. (2011). Evaporative enrichment of oxygen-18 and deuterium in lake waters on the Tibetan Plateau. *Journal of Paleolimnology*, *46*(2), 291–307. https://doi.org/10.1007/s10933-011-9540-y